



# Flood risk index mapping in data scarce region by considering GIS and MCDA (FRI mapping in data scarce region by considering GIS and MCDA)

S. K. Ray<sup>1</sup>

Received: 14 July 2023 / Accepted: 12 February 2024

© The Author(s), under exclusive licence to Springer Nature B.V. 2024

## Abstract

Climate change is responsible for triggering one of the most destructive natural disasters known as flooding. The flood risk index quantifies the vulnerability of an area to flooding, providing valuable insights for mitigation and preparedness efforts. Flood risk index integrates factors, aiding understanding and fostering resilient communities. This study uses an integrated strategy of geospatial technology and multi-criteria decision analysis to produce a map of the flood risk index for a data scarce region. Through this research work, fifteen thematic maps (i.e., Lithology, Soil, Slope, Drainage Density, Land use and Land cover, Rainfall, Distance from river, Permeability, Runoff, Normalized Difference Vegetation Index, Normalized Difference Built-up Index, Modified Normalized Difference Water Index, Topographic Wetness Index, Profile and Plan Curvature) in case of flood hazard index and three thematic maps (i.e., Population density, Crop production and Road river interaction) in case of flood vulnerability index were used. Thematic maps checked for multicollinearity, overlaid in ArcGIS with ranked assignments using AHP to develop flood hazard and vulnerability maps. The flood risk map was developed by integrating the flood hazard and vulnerability maps. The research region divided into five categories based on flood risk index map: very low (8%), low (28%), moderate (16%), high (20%), and very high (28%). The regions such as Vangara, Pathapatnam, Tekkali, Kusumala, Ichapuram shows very high tendency towards flood risk. This was due to favorable factors such as high/ moderate runoff, slope (very gentle/ gentle), very low/ low permeability, lithology (granite/ gneiss) etc. of the research region.

**Keywords** Flood Hazard Index · Multicollinearity · Flood Vulnerability Index · Analytical hierarchy process · Sensitivity analysis

---

✉ S. K. Ray  
sanjayitg632@gmail.com

<sup>1</sup> Civil Engineering Department, Aditya Institute of Technology and Management (AITAM), Srikakulam, Andhra Pradesh, India

# 1 Introduction

Floods are a naturally occurring phenomenon that affects human settlements and agricultural areas worldwide. While often associated with negative consequences, the presence of floods can result in environmentally sustainable benefits for areas that have been affected by prolonged droughts (Arya & Singh, 2021; Desalegn & Mulu, 2020). Floods, impacting numerous individuals worldwide, are amongst the most prevalent and catastrophic natural calamities that occur frequently, and their consequences are not limited to the loss of human lives but also result in significant economic and environmental damages (Abu El-Magd et al., 2020). Climate change is one of the major problem world is facing now a days. Due to climate change rainfall duration is slowly reducing and rainfall intensity is slowly increasing, as a result of that flood frequencies are increasing (Ehteram et al., 2022; Lai et al., 2022; Polong et al., 2023). According to the United Nations, floods are responsible for 70% of all natural disasters worldwide, and in the past few years, Floods have become more frequent and intense as a result of changes in the climate and activities by humans (Vörösmarty et al., 2005). Experts around the world have collaborated to conduct organized attempts to chart out the likelihood of floods and simulate flooding scenarios (Hussain et al., 2021; Ogato et al., 2020; Velasco et al., 2016). Floods are mostly caused by protracted periods of heavy, intense rainfall in a specific location. Insufficient capabilities of embankments, drainage channels, and waterways as well as improper disposal of solid waste, are significant factors contributing to early monsoon season floods (Arrighi, 2021; Singh et al., 2020).

Several researchers have utilized the Analytical Hierarchical Process (AHP) developed by Saaty (1987), in conjunction with the Geographic Information System (GIS), to conduct flood analysis (Amare & Okubay, 2019; Chen et al., 2018; Memon et al., 2020; Morea & Samanta, 2020; Yang et al., 2018). Accurately identifying the causative factors of floods is crucial due to their associated impacts. Flood risk mapping is a complex process that requires the integration of various data sources and analytical techniques. Several approaches have been proposed for flood risk mapping, including empirical, statistical, and physical models. The Flood Risk Index (FRI) map is designed to display various classes of seriousness zones based on predetermined characteristics and weights. This map has been developed using AHP and GIS datasets to provide accurate and reliable information. It is essential to understand that the FRI map's severity zones are determined according to the selected criteria and their corresponding weights. Identifying flood-prone areas and implementing measures to mitigate risks is crucial for disaster management, particularly in developing countries facing increasing climate change-related challenges (Chakraborty & Mukhopadhyay, 2019). While structural mitigation of flooding methods may require extensive ground elevation and cross-sectional data, non-structural approaches combined with geospatial data and the Multi-criteria Decision Analysis (MCDA) approach are commonly used to identify high-risk areas in regions with limited data. As a result, mapping flood risk areas has grown crucial for disaster planners to do effectively mitigate and manage the impact of disasters (Dayala et al., 2020; Merz et al., 2021; Nasiri et al., 2016; Rincon et al., 2018). The Srikakulam district near the coastal region of Andhra Pradesh, India, has experienced significant flooding, with occurrences in the years 1970, 1979, 1987, 1994, 1998, 2002, 2006, 2009, 2011, 2012, 2014, 2016, 2018, 2020, 2021 and 2022. This happens due to presence of two rivers i.e., Nagavali River and Vamsadhara River. Insufficient historical data is a considerable obstacle in flood analysis and the sustainable management of watersheds that are predisposed to flooding.

Despite the prevalence of flooding worldwide, there has been insufficient research conducted on data-poor sub-basins when it comes to analyzing flood data (Gandini et al., 2020). This includes critical information such as cross-sectional discharge data, satellite images of flood inundation, and observed flood marks from past events that can lead to flooding in developing nations. Empirical models are appropriate for areas with a lengthy history of flooding since they are based on previous flood information and statistical evaluation (Samela et al., 2018). However, in data-scarce regions, empirical models may not be effective due to the lack of adequate data. Statistical models use statistical techniques to analyze the relationship between flood variables and additional elements that raise the probability of flooding, such as rainfall, land use, and topography (Petroselli et al., 2019; Vojtek & Vojtekova, 2019). Statistical models are suitable for data-scarce regions as they require only a few key variables to predict flood risk. Physical models are based on the principles of hydraulics and hydrology and simulate the flood behavior of a river system (Baquedano & Ferreira, 2021; Martinez-Gomariz et al., 2021; Requena et al., 2018). Physical models require detailed data on river morphology and hydrological parameters, which may not be available in data-scarce regions.

GIS is an influential tool for geographical information analysis and management and has been widely used for flood risk mapping. GIS can integrate different data from various sources, such as topographic maps, land use maps, and rainfall data, and provide a spatially explicit representation of flood risk (Bonazza et al., 2018; Doorga et al., 2022; Ferreira & Santos, 2020; Gazi et al., 2019; Miranda & Ferreira, 2019; Quinn et al., 2019; Teng et al., 2017; Xiao et al., 2021). MCDA is an evaluative technique that can be utilized to assess the comparative significance of diverse criteria and sub-criteria in the context of flood risk assessment. MCDA can be used to assign weights to different flood risk factors and develop a composite flood risk index (Baquedano & Ferreira, 2021; Mundhe, 2019; Prieto et al., 2020; Samela et al., 2018).

Hydrological parameters, crucial in understanding the flow and behavior of water systems, benefit significantly from the integration of RS and GIS (Palacio-Aponte et al., 2022). RS technologies, such as thermal infrared imagery and radar, provide valuable data on soil moisture, river morphology, and precipitation patterns. GIS processes this information to model and simulate hydrological processes, contributing to the identification of potential flood risk zones and the development of effective floodplain management strategies (Hermas et al., 2021; Schroeder et al., 2016).

In disaster management and resilience planning, the collaboration between RS and GIS is a game-changer. The dynamic mapping capabilities of GIS, fueled by continuously updated RS data, empower authorities to make informed decisions during emergency response and recovery phases (Khosravi et al., 2019). By incorporating real-time RS observations into GIS, emergency responders can assess the evolving situation on the ground, optimize resource allocation, and implement targeted interventions to mitigate the impact of flooding events (Rincon et al., 2018; Shahabi et al., 2021).

The integration of RS and GIS in flood risk mapping represents a synergistic approach that harnesses the strengths of both technologies (Kienberger et al., 2009). This collaboration not only enhances the accuracy of flood risk assessments but also provides a holistic understanding of the complex interactions between various environmental factors. As the technology continues to advance, the RS-GIS partnership is poised to play an increasingly vital role in shaping resilient communities and mitigating the devastating consequences of flooding worldwide (Solomun et al., 2021; Vojtek & Vojtekova, 2019).

In areas where data is scarce, flood risk assessment and management become challenging owing to the inadequacy of necessary facts and information required for accurate

flood risk mapping (Amare & Okubay, 2019). To address this issue, Two commonly used technologies for mapping flood risk are GIS and MCDA, their integration can provide a comprehensive approach for evaluating and managing flood risk in data-scarce regions (Martinez-Gomariz et al., 2021; Morea & Samanta, 2020). The Geospatial technique was utilized to create the Flood Vulnerability Index (FVI) and Flood Hazard Index (FHI) for Andhra Pradesh's Srikakulam district in India. These indices were designed to assist local stakeholders and watershed managers in managing excessive water and drought situations. The criteria and sub-criteria for the Flood Risk Index (FRI) map were analyzed using the AHP and MCDA techniques (Abu El-Magd et al., 2020; Desalegn & Mulu, 2020; Xiao et al., 2021). Nonetheless, creating an inundation map of flood for a farming rural zone necessitates an extremely precise digital elevation model, stage-discharge information, and surveyed transverse profiles, which are not available in the current research region. Consequently, the current research work endeavored to produce a flood risk map utilizing the GIS-AHP method in the deficiency of these datasets.

The aim of this study is to create a FRI by utilizing 18 thematic maps in ArcGIS software and applying the AHP. This research stands out due to its utilization of a larger number of thematic maps, specifically 18, compared to the previous maximum of 10 to 12 maps. Furthermore, the study incorporates a thorough assessment of multicollinearity and sensitivity analysis. By including these checks and using a greater number of thematic maps, the accuracy of the FRI map is significantly enhanced. Consequently, the FRI map provides highly reliable data that can greatly contribute to effective long-term watershed management in flood-prone areas.

## 2 Materials and methods

### 2.1 Research region

The study conducted in the Srikakulam District of Andhra Pradesh focuses on the Nagavali and Vamsadhara fluvial systems within the coastal tracts. This particular research region spans approximately 5840 km<sup>2</sup>, located between latitudes 18° 40' N–18° 09' N and longitudes 84° 10' E–83° 39' E. The Nagavali and Vamsadhara rivers are two prominent river systems in northern Andhra Pradesh, distinctly marked by the Eastern Ghats, with a gradual slope from north to south. Originating from a hill near Lakhbahal village in the Kalahandi District of Odisha, the Nagavali river traverses through Nakrundi, Kerpai, Kalyansinghpur, and Rayagada in Odisha, before merging into the Bay of Bengal near Kallepalli village in Srikakulam, Andhra Pradesh. The total length of the Nagavali river is 256 km, with 160 km falling within Odisha and the remaining portion flowing through Andhra Pradesh. In contrast, the Vamsadhara river stretches for a distance of 254 km until it meets the Bay of Bengal at Kalingapatnam in Andhra Pradesh. The defined study region's Digital Elevation Model (DEM) is illustrated in Fig. 1.

### 2.2 Data procurement

In order to acquire the necessary data for the study, multiple sources were utilized to ensure access to reliable and diverse information. The 12.5 m resolution of DEM data was obtained from the Alaska Search Facility in Earth Data, which is conveniently accessible online at <https://search.asf.alaska.edu/#/>. Conversely, Landsat 8 data were sourced from

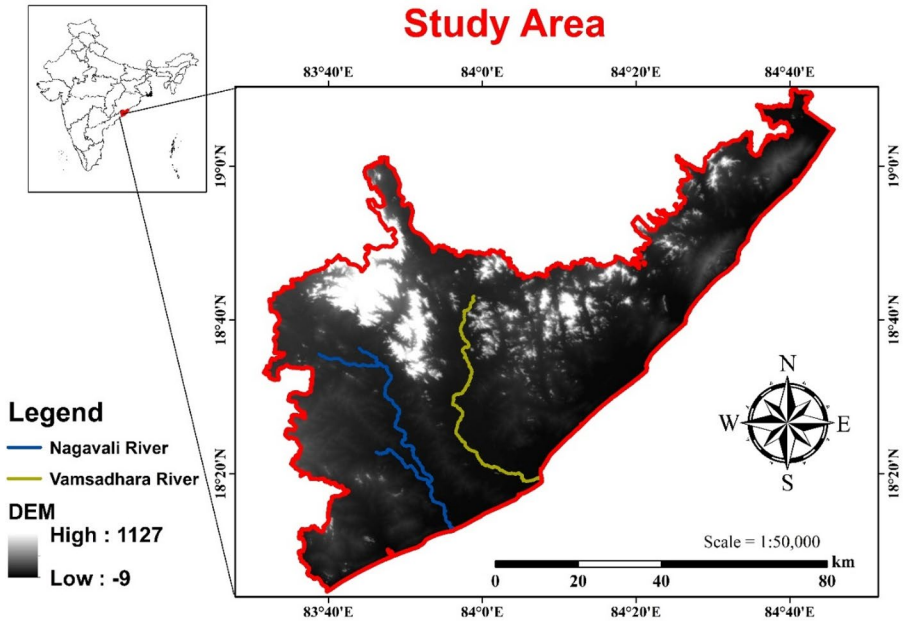


Fig. 1 DEM of the study area

Bhuvan, the National Remote Sensing Centre (NRSC), freely available at <http://bhuvan.nrsc.gov.in>. Rainfall data were acquired from the Center for Hydrometeorology & Remote Sensing (CHRS) and can be accessed at <https://chrsdata.eng.uci.edu/>. To gather information regarding lithology and road networks, data at a scale of 1:50,000 were procured from the Geological Survey of India (GSI), accessible at <https://bhukosh.gsi.gov.in/Bhukosh/Public>. The soil type and soil depth map, also at a scale of 1:50,000, were obtained from the National Atlas and Thematic Mapping Organization's district planning map series. Population density data were collected from the Census of India, National Statistical Office, while crop production data were procured from the Agricultural Department in Srikakulam, Andhra Pradesh.

## 2.3 Methodology

In order to effectively manage floods and minimize the impact on infrastructure and human lives, it is essential to identify the Flood Risk Index (FRI) map. The primary goal of current study is to evaluate the possible threat of flood risk in the Srikakulam district by employing spatial analytical tools and the AHP. By integrating flood vulnerability and hazard maps, the FRI was computed. The determination of main classes and sub-classes weights was based on an extensive literature review and expert input. In context to spatial resolution of map, the pixel size having matrix with 6344 columns and 5597 rows and a cell size of  $12.5 \text{ m} \times 12.5 \text{ m}$  was used for all the thematic maps. For conversion of pixel size, "Nearest Neighbor method" was used for discrete data (i.e., Lithology, Land Use and Land Cover (LULC), Distance from River (Dr), Population Density, Crop Production and Road River Interaction) whereas "Cubic method" was used for continuous data (i.e., Hydrological Soil

Group (HSG), Slope, Drainage Density (DD), Rainfall, Permeability, Runoff, Normalized Difference Vegetation Index (NDVI), Normalized Difference Built-up Index (NDBI), Modified Normalized Difference Water Index (MNDWI), Topographic Wetness Index (TWI), Profile and Plan curvature).

## 2.4 Development of FRI map

To generate the spatial database for the FRI map, various meteorological and topographical datasets were utilized. These datasets were then integrated with a GIS platform. The construction of the FRI map involved the consideration of a total of eighteen factors. These factors were carefully selected and analyzed to ensure a comprehensive assessment of flood risk. The present study employed fifteen thematic maps for Flood Hazard Index (FHI) determination. Additionally, three thematic maps, namely Population Density, Crop Production, and Road-River Interaction, were prepared for Flood Vulnerability Index (FVI) analysis. All of these maps were generated using ArcGIS software. To ensure the reliability of the analysis, a multicollinearity check was conducted on all 18 thematic maps. Subsequently, the thematic maps were overlaid in ArcGIS after allotting ranks and weights using the AHP. Sensitivity analysis was then performed for both the FHI and FVI maps. The FRI map for the research region was produced by utilizing the weighted sum technique in ArcGIS software to combine the FHI and FVI maps as shown in Eq. 1.

$$\text{FRI} = \text{FHI} \times \text{FVI} \quad (1)$$

To validate the map of FRI, the Receiver Operating Characteristic (ROC) curve was considered. This comprehensive approach, utilizing advanced GIS techniques and analytical methods, facilitated the development of an accurate and validated FRI map, which is crucial for effective flood management and mitigation strategies. The diagram illustrating the process of creating the FRI can be observed in Fig. 2.

## 2.5 Development of FHI map

During the development of the FHI map, determining the underlying reasons for flood hazards was of utmost importance. In this specific research, multiple factors were considered significant in creating the map. These factors include Runoff, Slope, LULC, Lithology, NDVI, MNDWI, NDBI, HSG, DD, Rainfall, Dr, TWI, Profile, and Plan Curvature. The selection of these factors was based on a thorough literature review and their relevance to the research region (Chen et al., 2018; Doorga et al., 2022; Hussain et al., 2021). The following sections were presented the comprehensive approach employed to generate the digital maps with spatial information for all the chosen variables.

## 2.6 Runoff map

Runoff refers to the movement of water, such as rainwater or melted snow, over the Earth's surface. It happens when the amount of precipitation is greater than the soil's ability to retain or absorb water. Instead, the excess water flows over the land, typically following the natural slope or topography, and collects in streams, rivers, lakes, or other bodies of water (Arya & Singh, 2021). Initially, the catchment area was partitioned into multiple sub-catchments based on Hydrological Soil Group (HSG). Subsequently, the catchment area was

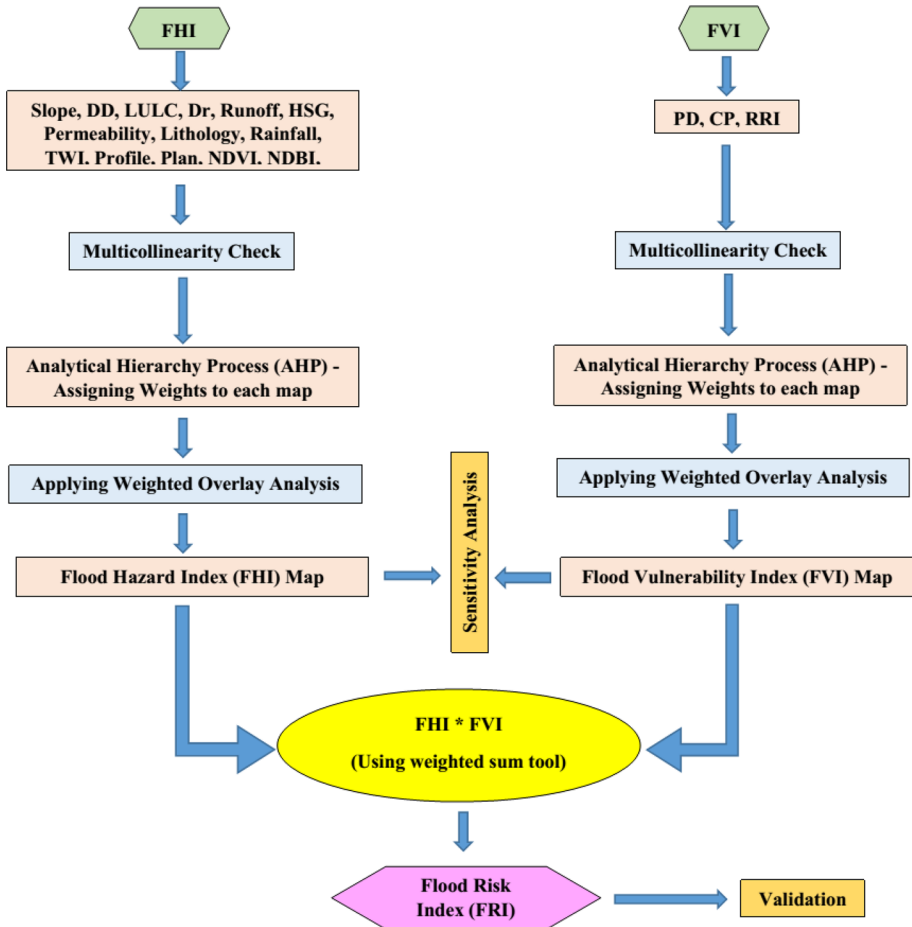


Fig. 2 Flowchart for delineating the FRI map

further divided into several sub-catchments based on drainage points. In every sub-catchment, the runoff depth was computed through the employment of the Soil Conservation Service (SCS) curve number technique. The estimation of runoff depth involves considering parameters such as curve number, HSG, rainfall, and LULC characteristics specific to the research region. In the framework of this investigation, the runoff map was sorted into four distinct groups based on the depth of the runoff. The method utilized for classifying these groups was the "Natural Break" technique in ArcGIS.

Within the runoff map, the sub-classes (ranging from 29 to 38 mm, 39 to 71 mm, 72 to 111 mm, and 112 to 145 mm) were allocated ranks from 1 to 9. To accomplish this, the reclassify function within the spatial analyst tool of ArcGIS software was utilized. The reclassification procedure involved assigning a rank of 1 to the lowest runoff values, while higher runoff values received higher ranks. This ranking scheme was based on the underlying principle that higher runoff poses a greater risk of flooding, thus deserving a higher rank, whereas lower runoff corresponds to a lower risk of flooding, warranting a lower rank.

## 2.7 Slope map

The slope affects surface runoff, which in turn affects groundwater recharge. To assess the slope characteristics in the research region, a Slope map was generated using the DEM (Amare & Okubay, 2019). The Spatial Analyst Tools in GIS software were utilized, selecting the Surface option to generate the slope map. Following the generation of the slope map, it was then divided into five distinct classifications based on the measured slope inclination in degrees. The classification method employed for these groups was the "Natural Break" technique within the ArcGIS framework.

The slope map was classified into sub-classes such as Very low, Low, Moderate, High, and Very High, which were assigned ranks ranging from 1 to 9. This reclassification process was accomplished using the reclassify function within the ArcGIS spatial analyst tool. The ranking scheme was determined based on the understanding that the slope of the surface plays a crucial part in influencing both surface runoff and infiltration rates. Steep or high slopes tend to result in rapid rainwater runoff due to increased velocity. Conversely, flat or low slopes are more susceptible to quick waterlogging or flooding situations and have higher rates of infiltration. Hence, the highest rank was given to the sub-class representing very low or flat slope, indicating a lower risk, while the sub-class representing very high slope received the lowest rank, signifying a higher risk.

## 2.8 LULC map

The LULC map provides a visual representation of various Land cover-use within the research region, including agricultural land, wetlands, forests, built-up areas and water bodies, among others (Bonazza et al., 2018). For this research, the Earth Explorer website was used to gather the maps of Landsat 8. Landsat 8 data were collected on 12th April, 2022 with 0% cloud cover. The spatial resolution of Landsat image used was 30 m by 30 m. The image was first classified into different sub-classes using supervised image classification followed by resampling in ArcGIS. During dry season the Landsat images were collected. For image classification, the band numbers of the blue, green, and red colors were adjusted from low to high values. The image classification tools were then utilized to classify the image according to various land types. Enhancing the training sample numbers for each land category increased the accuracy of the LULC map. As the study area is small, for each sub-classes a 50 training samples were selected. This research area underwent classification into five primary classes, namely Forest, Barren, Agricultural, Water Bodies, and Built-up. The method employed for classifying these groups was the "Land use unit" in the ArcGIS framework. Hence, a total of 250 training samples were selected. Polygons were used to obtain the samples. After preserving the samples of training, the Maximum Likelihood classification technique was utilized in ArcGIS software to develop the final LULC map. For validation purpose, for each categories 50 points were selected and using Error matrix, an overall accuracy of 86% and kappa coefficient of 0.84 were obtained.

Within the LULC map, various sub-classes such as Forest, Barren/Waste, Agricultural, Water bodies and Built-up were given ranks ranging from 1 to 9. The LULC plays a significant role in influencing hydrological processes, including precipitation, infiltration, base flow, interflow and evapotranspiration. Built-up, barren land and water bodies tend to be more susceptible to floodwater due to higher runoff, whereas agriculture and forests exhibit relatively lower runoff characteristics. As a result, water bodies were assigned the highest



rank, indicating their significant contribution to floodwater. This was followed by built-up areas and barren land cover, both of which possess increased vulnerability to flooding. Forest regions, on the other hand, were assigned the lowest rank, reflecting their ability to mitigate runoff through their vegetation and infiltration capacities.

## 2.9 Lithology map

The lithology map provides information about the different rock types present in the sub-surface of a research region (Rincon et al., 2018). In the current research, the lithology map specific to the research region was obtained from the GSI by utilizing the coordinate extents of the research region. To enhance the accuracy of the lithology map, additional information was gathered from the Central groundwater board (CGWB) situated in Visakhapatnam, Andhra Pradesh, India. Subsequently, this information was compared and authenticated with the lithology map procured from the GSI. Using the information gathered from the field, the lithographic map was corrected and improved. The predominant geological features within the research area can be classified into four distinct rock structures. The classification method employed for these groups utilized the "Lithological unit" in the ArcGIS platform.

Within the lithology map, different sub-classes such as Granite, Gneiss, Laterite, and Quartz were given ranks ranging from 1 to 9. This reclassification was performed using the reclassify function within the ArcGIS software's spatial analyst tool. Lithology, in combination with topography, plays a crucial role in influencing flooding patterns. For instance, when impermeable lithology underlie low-lying areas or valleys, they hinder drainage and contribute to water accumulation, thereby increasing the risk of flooding. Conversely, permeable lithology underlying elevated areas facilitate natural drainage and reduce the likelihood of flooding. Considering these factors, the highest rank was assigned to Granite due to its impermeability and favorable influence on flood. Gneiss received the second-highest rank, followed by Laterite and Quartz. This ranking scheme was based on the understanding that lithology with greater impermeability, such as Granite, have a positive impact on flood risk, while lithology with lower impermeability, such as Laterite and Quartz, have a comparatively lesser influence.

## 2.10 NDVI map

NDVI is an index commonly used in remote sensing and vegetation studies to assess the health, density, and vigor of vegetation cover (Martinez-Gomariz et al., 2021). NDVI was estimated by considering the red and near-infrared (NIR) bands of remote sensing imagery, typically obtained from satellites or aerial sensors. By applying Eq. 2 to the Landsat 8 imagery through the raster calculator function available in ArcGIS software, the NDVI map for the research region was prepared.

$$\text{NDVI} = \frac{\text{NIR} - \text{RED}}{\text{NIR} + \text{RED}} \quad (2)$$

The NDVI map was subdivided into five groups based on the NDVI values. The classification method employed for these groups was the "Equal Interval" technique within the ArcGIS platform. Within the NDVI map, various sub-classes such as Very Low, Low, Moderate, High, and Very High were assigned ranks varying from 1 to 9. This reclassification process was achieved using the reclassify function within the ArcGIS software's

spatial analyst tool. The NDVI is a measure that reflects the density and health of vegetation in an area. Negative value of NDVI generally represents the water, while positive value of NDVI represents the vegetation. The relationship between NDVI and flooding is inversely correlated. Higher value of NDVI represents a greater existence of healthy vegetation, which can contribute to better water absorption, reduced surface runoff, and increased infiltration capacity. Therefore, areas with higher NDVI values tend to have a lower probability of flooding. Based on this understanding, the highest rank was allocated to the Very Low NDVI sub-class, indicating a reduced flood risk, whereas the Very High NDVI sub-class assigned the lowest rank, suggesting a higher vulnerability to flooding.

## 2.11 NDBI map

NDBI is a remote sensing index commonly used to detect and quantify built-up areas within an urban or rural landscape (Ferreira & Santos, 2020). NDBI was derived from satellite or aerial imagery and is calculated using the NIR and short-wave infrared (SWIR) spectral bands. Equation 3, which refers to the formula for calculating the NDBI, was implemented using the Landsat 8 imagery through the raster calculator function in ArcGIS software. This process involved performing the necessary calculations on the respective spectral bands to derive the NDBI values for each pixel in the research region.

$$\text{NDBI} = \frac{\text{SWIR} - \text{NIR}}{\text{SWIR} + \text{NIR}} \quad (3)$$

The NDBI map underwent segmentation into five groups, categorized according to NDBI values. The classification method utilized for these groups was the "Equal Interval" technique within the ArcGIS platform. Within the NDBI map, different sub-classes such as Very Low, Low, Moderate, High, and Very High were assigned ranks varying from 1 to 9. This reclassification process was accomplished using the reclassify function within the ArcGIS software's spatial analyst tool. The NDBI is a measure that assesses the extent and density of built-up or urban areas in a region. Negative values of NDBI generally represents the existence of water bodies, whereas positive value of NDBI represents the existence of vegetation or built-up areas within urban settings. The relationship between NDBI and flooding is also inversely correlated. Higher NDBI values indicate a greater density of built-up areas, which can result in increased surface runoff and reduced infiltration capacity. Therefore, areas with higher NDBI values tend to have a higher probability of flooding. Conversely, lower NDBI values indicate the presence of water bodies or less dense urban areas, which typically have a lower risk of flooding. As a result, the ranking scheme was established, with the Very Low NDBI sub-class assigned the highest rank, indicating a lower probability of flooding, whereas the Very High NDBI sub-class allocated the lowest rank, suggesting a higher vulnerability to flooding.

## 2.12 MNDWI map

The MNDWI is a remote sensing index that is used in aerial or satellite photography to locate and map water bodies. MNDWI was particularly effective in differentiating water bodies from other land cover types, such as vegetation and built-up areas (Xiao et al., 2021). Equation 4, was used for estimating the MNDWI map by considering Landsat 8 image through raster calculator function in ArcGIS.

$$\text{MNDWI} = \frac{\text{GREEN} - \text{SWIR}}{\text{GREEN} + \text{SWIR}} \quad (4)$$

The MNDWI map was divided into five groups based on MNDWI values. The classification method employed for these groups was the "Equal Interval" technique within the ArcGIS platform. Within the MNDWI map, different sub-classes such as Very Low, Low, Moderate, High, and Very High were assigned ranks varying from 1 to 9. This reclassification process was conducted using the reclassify function within the ArcGIS software's spatial analyst tool. The MNDWI is a remote sensing index that helps identify water bodies based on the spectral properties of the imagery. Negative values of MNDWI generally represents the existence of vegetation, whereas positive values of MNDWI represents the existence of water bodies. In contrast to the previous indices discussed, the relationship between MNDWI and flooding is directly correlated. Higher MNDWI values suggest a greater presence of water bodies, indicating a higher flooding probability. This is because regions with higher values of MNDWI are more likely to have increased surface runoff and reduced infiltration capacity, which contribute to flood risk. Consequently, the ranking scheme was established, with the Very Low MNDWI sub-class assigned the lowest rank, indicating a lower probability of flooding, while the Very High MNDWI sub-class allocated the highest rank, indicating a higher vulnerability to flooding.

### 2.13 HSG map

The penetration and seepage velocities from the top layer to the underground, encompassing water-bearing layers, are largely impacted by the constitution of the Soil. The HSG has been sorted into four groups by the United States Department of Agriculture (USDA), which are A, B, C, and D (Teng et al., 2017). To represent these soil groups, a new shapefile was created, and polylines were drawn based on the soil groups considering the editor tool in present in the ArcGIS. The attribute table was then utilized to assign the corresponding soil groups to the generated polygons by joining the polylines. A map of the soil was created by consolidating the polygons belonging to identical soil groups in the attribute table with the use of the editor tool.

Within the research region, the prevalent soil groups were categorized into four types. The classification method employed for these groups was the "Soil group unit" technique within the ArcGIS platform. Within the HSG map, the different sub-classes, namely A, B, C, and D, were allocated ranks ranging from 1 to 9. This reclassification process was performed using the reclassify function within the ArcGIS software's spatial analyst tool. The soil types present in an area plays a critical part in determining its susceptibility to flooding. The capacity of the soil to hold water and its ability to absorb water into its layers have a significant effect on the extent of flooding. In this regard, the ranking scheme was established. The highest rank was assigned to Group D soil due to its low infiltration rate, indicating a higher potential for surface runoff and reduced infiltration capacity. Following that, Group C soil received the next highest rank due to its moderate infiltration capacity. Group B soil was assigned a lower rank than Group C due to its higher infiltration capability. Lastly, Group A soil, characterized by very high infiltration capacity, was assigned the lowest rank. This ranking reflects the relationship between soil type and flood susceptibility, with Group D being the most vulnerable to flooding and Group A being the least susceptible due to its high infiltration capacity.

## 2.14 DD map

The density of drainage is a significant parameter that indicates the spacing and composition of stream channels, offering insights into the mean stream channel length throughout the entire basin (Yang et al., 2018). In order to generate the DD map for the research region, the DEM was utilized. The process involved selecting the "Hydrology" option within the "Spatial Analyst Tools" in ArcGIS software. Initially, DEM was referenced geographically and transformed to a projected coordinate system. Then, the map of flow direction was produced, which was succeeded by the development of the map of flow accumulation. To ensure accuracy, values less than 500 pixels in the flow accumulation map were excluded. The stream system of the research region was subsequently produced utilizing the flow direction and flow accumulation maps. By utilizing the produced stream network, the stream hierarchy of the sub-basin was established. Furthermore, the line density feature in ArcGIS software was utilized to create the DD map.

The DD map illustrates the concentration of drainage in the research area, segmented into five classifications. The classification method employed for these groups was the "Equal Interval" technique within the ArcGIS platform. Within the DD map, different sub-classes such as Very Low, Low, Moderate, High, and Very High were assigned ranks varying from 1 to 9. This reclassification process was carried out using the reclassify function within the ArcGIS software's spatial analyst tool. There exists an inverse relationship between flood hazard and DD. Higher values of DD indicate a lower risk of flooding, while lower values of DD indicate a higher flood risk. Therefore, DD plays a crucial role in generating the FHI map. In light of this relationship, a ranking scheme was established. A high DD, indicating a higher potential for efficient drainage and reduced flood risk, was assigned a low rank. On the other hand, a low DD, indicating a lower ability for efficient drainage and a higher flood risk, was assigned a high rank. By incorporating DD into the analysis, the resulting FHI map benefits from this vital information, enabling a comprehensive assessment of flood hazards.

## 2.15 Rainfall map

Surface runoff is significantly influenced by rainfall, making it a vital natural resource (Memon et al., 2020; Ray, 2023). In this study, precipitation data covering a time frame of three decades (1993–2022) was gathered from various rain gauges operated by the Indian Meteorological Department (IMD) located in the vicinity and adjacent areas of the study site's buffer zone. To examine the geographical arrangement of precipitation, an ArcGIS software was utilized to generate a map displaying the distribution of rainfall. Initially, the annual average rainfall data for all the rain gauges was estimated in Excel. Afterwards, the information was integrated into ArcGIS utilizing the latitude and longitude coordinates of the precipitation measuring devices. In order to display the spatial arrangement, an interpolation technique known as Inverse Distance Weight (IDW) was executed in ArcGIS, leading to the development of the rainfall map for the designated study area.

The rainfall map was categorized into five distinct groups. The classification technique utilized for these groups was the "Natural Break" method within the ArcGIS platform. Within the map, different sub-classes representing specific rainfall ranges, such as 918–1043 mm, 1044–1100 mm, 1101–1158 mm, 1159–1222 mm, and 1223–1342 mm, were assigned ranks ranging from 1 to 9. This reclassification process was performed

using the reclassify function within the ArcGIS software's spatial analyst tool. Infiltration, which refers to the process of water seeping into the soil, is affected by mainly two key parameters: intensity and duration of rainfall. Higher intensity combined with shorter duration leads to increased runoff, while lower intensity coupled with longer duration results in decreased runoff. There exists a strong linear positive relationship between floods and rainfall. Regions experiencing high rainfall were assigned a high rank, indicating a greater likelihood of flooding, while areas with less rainfall were allocated a lesser rank, suggesting a lower flood risk. This ranking scheme reflects the influence of rainfall on the runoff process and its impact on flood occurrence. Regions with higher rainfall amounts are more susceptible to floods due to increased runoff, while regions with lower rainfall amounts are less prone to flooding due to reduced runoff.

## 2.16 Distance from river map

With the aid of the ArcGIS program, a map indicating the distance from the river was created for the study area. The procedure consisted of various stages. At first, the flow accumulation was modified to a threshold of 500 pixels by utilizing the map algebra function in the spatial analyst tool. Subsequently, the stream network was produced. To formulate the distance from river map, the multi-ring buffer function was employed, which was based on the distances that were calculated (Singh et al., 2020).

The research area underwent division into six distinct groups based on distances. The classification method utilized for these groups was the "Manual" technique within the ArcGIS platform. Within this map, different sub-classes representing specific distance ranges from the river, such as 500 m, 1000 m, 2000 m, 3000 m, and distances greater than 3000 m, were assigned ranks ranging from 1 to 9. This reclassification process was performed using the reclassify function within the ArcGIS software's spatial analyst tool. The distance from a river has a significant influence on flood hazard and infiltration. Areas located closer to the river generally experience higher flood hazards and greater infiltration rates. On the other hand, areas farther away from the river tend to have lower flood hazards and reduced infiltration. As a result, higher ranks were assigned to areas in close proximity to the river, indicating a higher flood hazard and infiltration potential. Conversely, lower ranks were assigned to areas located farther away from the river, indicating a decreased flood hazard and infiltration potential. This ranking scheme captures the relationship between the distance from the river and the associated flood risk. Areas closer to the river are more susceptible to flooding due to their proximity, which can lead to higher flood hazards and infiltration rates. In contrast, areas located at greater distances from the river are generally less prone to flooding, resulting in reduced flood hazards and infiltration.

## 2.17 Permeability map

Permeability of soil refers to its ability to allow the movement of water or other fluids through its pores or spaces. It is a crucial property that affects the drainage and infiltration characteristics of soil (Dayala et al., 2020; Velasco et al., 2016). The permeability map was prepared by considering soil map and lithology map of the research region. Both maps were overlapped in the ArcGIS by assigning weightage to each thematic maps as well as its sub-classes by considering AHP. The permeability map was segmented into four categories. The classification method used for these groups was the "Equal Interval" technique within the ArcGIS platform. Within this map, different sub-classes representing varying

levels of permeability, such as Low, Moderate, High, and Very High, were assigned ranks varying from 1 to 9. This reclassification process was conducted using the reclassify function within the ArcGIS software's spatial analyst tool. Permeability refers to the soil's capacity to allow the movement of water or other fluids through its pores or spaces. It is a crucial characteristic that significantly influences the drainage and infiltration properties of the soil. In the context of flood susceptibility, permeability and flood are inversely related. Soils with low permeability tend to impede water movement, leading to increased surface runoff and higher flood potential. Conversely, soils with high permeability facilitate the movement of water, enhancing drainage and reducing the likelihood of flooding. Therefore, a high rank was assigned to areas with low permeability, indicating reduced water movement and higher flood susceptibility. Conversely, a low rank was assigned to areas with high permeability, indicating enhanced water movement and lower flood susceptibility.

## 2.18 TWI map

ArcGIS was used to build the TWI map. Initially, the slope map was prepared utilizing the spatial analyst tool, and afterward Eq. 5 was employed in the raster calculator feature, utilizing map arithmetic, to produce the TWI map (Ray, 2023). The equation incorporates the upslope ( $\alpha$ ) and topographic gradient ( $\beta$ ) parameters.

$$TWI = \ln \frac{\alpha}{\tan \beta} \quad (5)$$

The research area's TWI map underwent categorization into five groups. The classification approach employed for these divisions was the "Equal Interval" technique, implemented within the ArcGIS platform. Sub-classes within the TWI map, such as very high, high, moderate, low, and very low, were allocated ranks ranging from 1 to 9. This reclassification process was performed using the reclassify function within the ArcGIS software's spatial analyst tool. The TWI provides an indication of wetness within a landscape based on topographic characteristics. In general, areas with a low TWI, such as hilly and mountainous regions with steep slopes, tend to experience high runoff and are considered low-risk zones for flooding. On contrast, regions with a higher values of TWI, such as flat regions with gentle slopes, exhibit low runoff and are associated with a higher risk of flooding. Consequently, higher ranks were allocated to regions with higher values of TWI, representing flatter regions with lower runoff potential and a higher risk of flooding. Conversely, lower ranks were allocated to regions with lower TWI values, representing hilly or mountainous areas with steeper slopes and a lower risk of flooding.

## 2.19 Profile and plan curvature map

The profile curvature denotes the orientation of the highest incline, which is identical to it (Amare & Okubay, 2019). The map of profile curvature for the current study region was produced in ArcGIS by utilizing the curvature function in the 3D analyst tool. The plan curvature indicates the curvature that is at right angles to the direction of the steepest slope (Quinn et al., 2019). The map of plan curvatures for the current study site was produced in ArcGIS by utilizing the 3D analyst tool's curvature feature.

The categorization of the profile and plan curvature map involved dividing it into three groups. The classification method applied to these groups was the "Equal Interval" technique within the ArcGIS platform. Each sub-categories of the profile and plan curvature

maps, namely low, moderate, and high, were allocated ranks varying from 1 to 9, with ranks of 1, 5, and 9 respectively. The classification was accomplished through the utilization of the reclassify feature present in the spatial analyst tool embedded in the ArcGIS. In general, water exhibits a deceleration trend towards convex surfaces and an accumulation trend towards concave surfaces. A convex surface is inversely related to flooding, while a concave surface has a direct relationship with flooding. Consequently, a higher rank was assigned to the high sub-classes, representing concave surfaces, while a lower rank was assigned to the low sub-classes, representing convex surfaces.

## 2.20 Development of FVI map

The selection of parameters was based on a number of literature review, considering their significance in the domain of flood vulnerability as well as data availability. To conduct the flood vulnerability analysis, distinctive parameters were chosen. The social parameter was determined as the population density (number of individuals per square kilometer), the economic parameter as cropland productivity (kilograms per hectare), and the physical transportation parameter as the density of road-river intersection points per unit area (Arya & Singh, 2021; Bonazza et al., 2018; Chen et al., 2018; Gandini et al., 2020; Hussain et al., 2021; Requena et al., 2018). These indicators were deemed relevant and appropriate for assessing flood vulnerability in the research region.

## 2.21 Crop production map

The region's industrial and economic sectors heavily rely on agriculture, which highlights the importance of the proportion of cropland. This parameter is crucial when calculating the economic losses incurred by the region due to disasters (Prieto et al., 2020). To obtain data on the mean crop production in a year for the research region, information was collected from the Agricultural Department in Srikakulam, Andhra Pradesh, India. The mean yields of all currently grown crops in the research region were aggregated to determine the aggregate yield of crop per hectare for that specific tehsil.

A Crop Production Map was generated, categorizing the tehsil-wise total yield into five ranges. The classification method utilized for these ranges was the "Equal Interval" technique within the ArcGIS platform. Within the crop production map, sub-classes representing different yield ranges, namely 2389–3089, 3090–3970, 3971–4952, 4953–5808, and 5809–6403 kg per ha, were assigned ranks ranging from 1 to 9. This ranking was achieved using the reclassify function in the spatial analyst tool within ArcGIS software. In accordance with flood vulnerability, higher crop productions were assigned the highest rank, indicating greater susceptibility to flooding. Conversely, lower crop productions were assigned the least rank, indicating lower vulnerability to flood hazards.

## 2.22 Population density map

The population factor holds significant importance in conducting a comprehensive flood vulnerability study. This particular factor plays a crucial part in determining the vulnerable locations to social losses and damages caused by floods (Doorga et al., 2022). To gather the necessary population data for the research region, the Census of India for the year 2021 was utilized. Considering population as a vital element allows for a comprehensive evaluation of the impact

on the community in flood vulnerable areas due to flood-related events. The population density map was prepared in ArcGIS software by considering tehsil-wise population density.

The population density map underwent classification into five categories. The classification method employed for these groups was the "Equal Interval" technique within the ArcGIS platform. Within this map, different sub-classes representing population density ranges, namely 214–515, 515.1–653, 653.1–797, 797.1–1064, and 1064.1–1276 persons per sq. km., were assigned ranks ranging from 1 to 9. These rankings were assigned using the reclassify function within the spatial analyst tool in ArcGIS software. Considering flood vulnerability, the highest rank was assigned to areas with high population density, indicating their greater susceptibility to flooding. Conversely, lower ranks were allocated to regions with lower population density, indicating their lower vulnerability to flood hazards.

### 2.23 Road river intersection map

Road-river intersections were recognized as high-risk zones when it comes to flood occurrences. The impact of waterlogging at these junctions was demonstrated through an examination of the frequency of road-river intersections per unit area in the research region (Merz et al., 2021). The road network for the area of study was established using information related to road network using the GSI as a reference point. To build the shapefiles of the road and river networks, ArcGIS's intersection function was used, followed by the utilization of the point density tool to analyze the intersection points.

The map depicting road-river interactions was divided into four categories. The classification method applied to these groups was the "Natural Break" technique within the ArcGIS platform. Within this map, different sub-classes representing road river intersection densities, specifically 0–2, 3–5, 6–8, and 9–11 points per sq. km., were assigned ranks ranging from 1 to 9. These rankings were determined using the reclassify function within the spatial analyst tool of ArcGIS software. Considering flood vulnerability, the highest rank was assigned to regions with a high density of road river intersections, indicating their greater susceptibility to flooding. Conversely, lower ranks were assigned to areas with lower road river intersection densities, implying their lower vulnerability to flood hazards.

### 2.24 Multicollinearity checks for FHI and FVI

Multicollinearity is a statistical issue that occurs when one or more input variables in a model are highly correlated with each other. This can lead to challenges in accurately estimating the output of the model. Hence, prior to implementing a regression model, it is crucial to evaluate the multicollinearity between the input variables. (Montgomery et al., 2013; Ray, 2023). The variance inflation factor (VIF) and tolerance factor are two frequently used metrics for assessing multicollinearity. The tolerance was calculated using Eq. 6, while the VIF was calculated using Eq. 7. These measures help assess the extent of multicollinearity present in the model and guide further analysis and decision-making.

$$\text{Tolerance of the } i^{\text{th}} \text{ parameter } (T_i) = 1 - R_i^2 \quad (6)$$

$$\text{VIF of the } i^{\text{th}} \text{ parameter } (VIF_i) = \frac{1}{T_i} \quad (7)$$



To evaluate the existence of multicollinearity within the thematic maps, a random sample of 500 points was chosen from the research region. The data was extracted using ArcGIS and analyzed through the Statistical Package for Social Science (SPSS) to identify any multicollinearity concerns. Multicollinearity is deemed problematic if the tolerance value is below 0.10 or if the VIF is equal to or greater than 10. This examination assists in recognizing any significant correlations among the thematic maps, which could impact the dependability and precision of the regression model's outcomes.

**2.25 AHP for FHI and FVI**

AHP, a methodology developed by Prof. Thomas L. Saaty in 1987, offers a unique approach for evaluating the appropriateness of structures in their designated places. It utilizes the concept of MCDA. The AHP approach makes use of a collection of reciprocal matrices to compare different variables (Saaty, 1987, 1990, 2008). The importance of FHI and FVI is measured on a scale of 1 to 9 to establish a ranking. A rating of '1' indicates a restricted area where flood occurrence is very low, while a '9' signifies an exceptional zone for FHI and FVI which indicates high risk of flood. To evaluate the consistency of weights and ranks assigned to different thematic maps and their sub-classes, the 'Consistency Ratio (CR)' is estimated by considering Eq. 8, as suggested by Saaty (1990). If the CR is equal to or less than 0.1, It signals a decision to move on with the AHP evaluation that is appropriate, according to Saaty (1990).

$$\text{Consistency Ratio(CR)} = \frac{\text{CI}}{\text{RCI}} \tag{8}$$

$$\text{Consistency Index, CI} = \frac{\lambda_{\text{max}} - n}{n - 1} \tag{9}$$

where RCI stands for random consistency index, which is a pre-determined value by considering on the number of criteria being considered, n represents the number of thematic maps, and  $\lambda_{\text{max}}$  represents principal Eigen value, which is obtained through the Eigen value analysis of the pairwise comparison matrix.

**2.26 Overlay analysis for FHI and FVI**

Following the allocation of weights and rankings to every thematic map and their respective subcategories, the FHI and FVI maps were generated through a weighted overlay analysis conducted on ArcGIS software, specifically by utilizing the Spatial Analyst tool (Desalegn & Mulu, 2020). The formula for the overlay analysis as shown in Eq. 10 combines the different thematic maps based on their weights to calculate the final index value for each location:

$$\text{FHI or FVI} = \sum_{i=1}^n (W_i \times R_i) \tag{10}$$

where  $W_i$  stands for weight of the thematic map and  $R_i$  stands for rank of sub-classes. By multiplying each thematic map with its corresponding weight and summing up these weighted values, the overlay analysis produces the FHI and FVI maps. These maps provide an integrated representation of the hazard and vulnerability factors considered in the flood assessment analysis.

## 2.27 Sensitivity analysis for FHI and FVI

The sensitivity analysis unveils the influence of individual input thematic maps on the output thematic map. In the current research work, two distinct approaches were employed for sensitivity analysis, namely single parameter and map removal. To quantify the sensitivity, the Sensitivity Index (SI) was computed using Eq. 11 in the map removal sensitivity analysis (Ray, 2023). This index allows for the estimation of the extent to which the removal of a particular map affects the overall analysis results.

$$SI = \frac{\left| \left( \frac{FHI_{or} FVI}{N} \right) - \left( \frac{FHI'_{or} FVI'}{n} \right) \right|}{FHI_{or} FVI} \times 100 \quad (11)$$

In the context of the sensitivity analysis, the terms  $FHI'_{or} FVI'$  represent modified versions of FHI or FVI, respectively, where one thematic map is excluded at a time. The variable 'n' represents the total number of thematic maps considered to create  $FHI'_{or} FVI'$ , while 'N' represents the total number of thematic maps utilized to prepare the original FHI or FVI. In the single parameter sensitivity analysis, the weight factor (W) is determined using Eq. 12. This equation allows for the estimation of the influence of individual parameters on the overall analysis results.

$$W = \frac{P_r P_w}{FHI_{or} FVI} \times 100 \quad (12)$$

where  $P_r$  represents thematic map rank,  $P_w$  represents thematic map weight and FHI or FVI is flood hazard index or flood vulnerability index computed by using all of the thematic maps.

## 3 Results

All the fifteen thematic maps i.e., Runoff, Slope, LULC, Lithology, NDVI, NDBI, MNDWI, HSG, DD, Rainfall, Distance from River, Permeability, TWI, Profile, and Plan Curvature, were developed for preparation of FHI map. In addition to this, three more thematic maps i.e., population density, crop production and road river interaction, were prepared for FVI map. Finally, both FHI and FVI maps were multiplied in order to develop the FRI map (Table 1).

### 3.1 Multicollinearity checks for FHI and FVI

Presented in Tables 2 and 3 are the parameters from the investigation on multicollinearity concerning FHI and FVI. The outcomes reveal that all the thematic maps exhibit VIF values below the prescribed upper limit of 10, and their tolerance values surpass the designated lower threshold of 0.1. Consequently, based on the aforementioned findings, it becomes apparent that no detectable issue of multicollinearity exists among the evaluated thematic maps.

**Table 1** Details of literature review for FRI

SI No	Literature	Multicollinearity Check	Sensitivity Analysis	No. of Thematic Maps	Accuracy
1	Abu El-Magd et al. (2020)	No	No	8	0.73
2	Amare and Okubay (2019)	No	No	6	0.73
3	Arrighi (2021)	No	No	12	0.74
4	Arya and Singh (2021)	No	No	7	0.77
5	Baquedano and Ferreira (2021)	No	No	8	0.76
6	Bonazza et al. (2018)	No	No	7	0.75
7	Chakraborty and Mukhopadhyay (2019)	No	No	6	0.75
8	Chen et al. (2018)	No	No	7	0.74
9	Dayala et al. (2020)	No	No	6	0.77
10	Desalegn and Mulu (2020)	No	No	10	0.76
11	Doorga et al. (2022)	No	No	8	0.75
12	Ferreira and Santos (2020)	No	No	12	0.73
13	Gandini et al. (2020)	No	No	9	0.74
14	Gazi et al. (2019)	No	No	7	0.73
15	Hussain et al. (2021)	No	No	12	0.75
16	Martinez-Gomariz et al. (2021)	No	No	8	0.77
17	Memon et al. (2020)	No	No	11	0.76
18	Merz et al. (2021)	No	No	10	0.75
19	Miranda and Ferreira (2019)	No	No	9	0.74
20	Morea and Samanta (2020)	No	No	10	0.74
21	Mundhe (2019)	No	No	11	0.73
22	Ogato et al. (2020)	No	No	12	0.76
23	Petroselli et al. (2019)	No	No	11	0.77
24	Prieto et al. (2020)	No	No	8	0.77
25	Quinn et al. (2019)	No	No	6	0.76
26	Requena et al. (2018)	No	No	6	0.75
27	Rincon et al. (2018)	No	No	6	0.75
28	Samela et al. (2018)	No	No	7	0.73
29	Singh et al. (2020)	No	No	7	0.74
30	Teng et al. (2017)	No	No	10	0.74
31	Velasco et al. (2016)	No	No	7	0.76
32	Vojtek and Vojtekova (2019)	No	No	8	0.77
33	Xiao et al. (2021)	No	No	7	0.74

### 3.2 AHP for FHI and FVI

To determine the weightage for every thematic map and their sub-categories, the AHP method was employed. For FHI, Tables 4 and 5 display the pairwise comparison matrix and the corresponding normalized pairwise comparison matrix for the research region. Similarly, for FVI, Tables 6 and 7 demonstrate the respective pairwise comparison matrix and normalized pairwise comparison matrix. The values in the normalized pairwise comparison matrix were calculated by dividing the value of each cell by the column total value.

**Table 2** Collinearity statistics for all the parameters of FHI

Sl. No	Thematic maps	Tolerance	VIF
1	Runoff	0.562	1.78
2	Slope	0.612	1.63
3	LULC	0.553	1.81
4	Lithology	0.638	1.57
5	NDVI	0.941	1.06
6	NDBI	0.922	1.08
7	MNDWI	0.821	1.22
8	HSG	0.914	1.09
9	Drainage density	0.953	1.05
10	Rain fall	0.924	1.08
11	Distance from river	0.716	1.40
12	Permeability	0.891	1.12
13	TWI	0.751	1.33
14	Plan curvature	0.658	1.52
15	Profile curvature	0.638	1.57

**Table 3** Collinearity statistics for all the parameters of FVI

Sl. No	Thematic maps	Tolerance	VIF
1	Crop production	0.68	1.47
2	Road river interaction	0.57	1.75
3	Population density	0.46	2.17

The criteria weights were obtained by averaging the values in each row. Consistency computation for the pairwise comparison matrix was conducted using Eqs. 8 and 9. For FHI, the consistency index and consistency ratio were determined as 0.06 and 0.04, respectively. In the case of FVI, the values were 0.02 and 0.03, respectively. Since the consistency ratio values of 0.06 and 0.02 are less than 0.1, it can be concluded that the pairwise comparison matrices are consistent. Thus, the weights estimated through Table 5 and 7 can be utilized to assign weights to all the thematic maps. Table 8 presents the weight and rank values for all the thematic maps concerning FHI, while Table 9 displays the corresponding values for FVI. In order to enhance accuracy, the sub-classes of each thematic maps were assigned ranks based on their priority level, considering expert opinion and literature review.

### 3.3 Development of FHI

#### 3.3.1 Runoff map

The weighting process in accordance with the AHP assigned a weight of 16.4% to the runoff map. Within the context of this study, the map depicting runoff was categorized into four distinct groups according to the depth of the runoff. These categories are defined as (29–38) mm, (39–71) mm, (72–111) mm, and (112–145) mm. The corresponding areas occupied by each category within the research region are approximately 24%, 26%, 29%, and 21%, respectively. Figure 3 depicts the runoff map for the research region.

**Table 4** Pairwise comparison matrix for FHI

Maps	R	SI	LULC	Li	NDVI	NDBI	MNDWI	HSG	DD	R/f	Dr	P	TWI	Pc	Plc
R	1.00	1.00	2.00	2.00	3.00	3.00	3.00	4.00	4.00	5.00	5.00	6.00	6.00	7.00	7.00
SI	1.00	1.00	2.00	2.00	3.00	3.00	3.00	4.00	4.00	5.00	5.00	6.00	6.00	7.00	7.00
LULC	0.50	0.50	1.00	1.00	2.00	2.00	2.00	3.00	3.00	4.00	4.00	5.00	5.00	6.00	6.00
Li	0.50	0.50	1.00	1.00	2.00	2.00	2.00	3.00	3.00	4.00	4.00	5.00	5.00	6.00	6.00
NDVI	0.33	0.33	0.50	0.50	1.00	1.00	1.00	2.00	2.00	3.00	3.00	4.00	4.00	5.00	5.00
NDBI	0.33	0.33	0.50	0.50	1.00	1.00	1.00	2.00	2.00	3.00	3.00	4.00	4.00	5.00	5.00
MNDWI	0.33	0.33	0.50	0.50	1.00	0.50	1.00	2.00	2.00	3.00	3.00	4.00	4.00	5.00	5.00
HSG	0.25	0.25	0.33	0.33	0.50	0.50	0.50	1.00	1.00	2.00	2.00	3.00	3.00	4.00	4.00
DD	0.25	0.25	0.33	0.33	0.50	0.33	0.50	1.00	1.00	2.00	2.00	3.00	3.00	4.00	4.00
R/f	0.20	0.20	0.25	0.25	0.33	0.33	0.33	0.50	0.50	1.00	1.00	2.00	2.00	3.00	3.00
Dr	0.20	0.20	0.25	0.25	0.33	0.33	0.33	0.50	0.50	1.00	1.00	2.00	2.00	3.00	3.00
P	0.17	0.17	0.20	0.20	0.25	0.25	0.25	0.33	0.33	1.00	1.00	1.00	1.00	2.00	2.00
TWI	0.17	0.17	0.20	0.20	0.25	0.25	0.25	0.33	0.33	1.00	1.00	1.00	1.00	2.00	2.00
Pc	0.14	0.14	0.17	0.17	0.20	0.20	0.20	0.25	0.25	1.00	1.00	1.00	1.00	1.00	1.00
Plc	0.14	0.14	0.17	0.17	0.20	0.20	0.20	0.25	0.33	0.33	0.50	0.50	1.00	1.00	1.00
CT	5.52	5.52	9.40	9.40	15.57	14.90	15.57	24.17	24.25	36.33	36.50	47.50	48.00	61.00	61.00

**Table 5** Normalized pairwise comparison matrix for FHI

Maps	R	SI	LULC	Li	NDVI	NDBI	MNDWI	HSG	DD	R/f	Dr	P	TWI	Pc	Plc	Criteria Weight
R	0.18	0.18	0.21	0.21	0.19	0.20	0.19	0.17	0.16	0.14	0.14	0.13	0.13	0.11	0.11	16.4
SI	0.18	0.18	0.21	0.21	0.19	0.20	0.19	0.17	0.16	0.14	0.14	0.13	0.13	0.11	0.11	16.4
LULC	0.09	0.09	0.11	0.11	0.13	0.13	0.13	0.12	0.12	0.11	0.11	0.11	0.10	0.10	0.10	11.1
Li	0.09	0.09	0.11	0.11	0.13	0.13	0.13	0.12	0.12	0.11	0.11	0.11	0.10	0.10	0.10	11.1
NDVI	0.06	0.06	0.05	0.05	0.06	0.07	0.06	0.08	0.08	0.08	0.08	0.08	0.08	0.08	0.08	7.2
NDBI	0.06	0.06	0.05	0.05	0.06	0.07	0.06	0.08	0.08	0.08	0.08	0.08	0.08	0.08	0.08	7.2
MNDWI	0.06	0.06	0.05	0.05	0.06	0.03	0.06	0.08	0.08	0.08	0.08	0.08	0.08	0.08	0.08	7.2
HSG	0.05	0.05	0.04	0.04	0.03	0.03	0.03	0.04	0.04	0.06	0.05	0.06	0.06	0.07	0.07	4.6
DD	0.05	0.05	0.04	0.04	0.03	0.02	0.03	0.04	0.04	0.06	0.05	0.06	0.06	0.07	0.07	4.6
R/f	0.04	0.04	0.03	0.03	0.02	0.02	0.02	0.02	0.02	0.03	0.03	0.04	0.04	0.05	0.05	3.1
Dr	0.04	0.04	0.03	0.03	0.02	0.02	0.02	0.02	0.02	0.03	0.03	0.04	0.04	0.05	0.05	3.1
P	0.03	0.03	0.02	0.02	0.02	0.02	0.02	0.01	0.01	0.03	0.03	0.02	0.02	0.03	0.03	2.3
TWI	0.03	0.03	0.02	0.02	0.02	0.02	0.02	0.01	0.01	0.03	0.03	0.02	0.02	0.03	0.03	2.3
Pc	0.03	0.03	0.02	0.02	0.01	0.01	0.01	0.01	0.01	0.03	0.03	0.02	0.02	0.02	0.02	1.7
Plc	0.03	0.03	0.02	0.02	0.01	0.01	0.01	0.01	0.01	0.01	0.01	0.01	0.02	0.02	0.02	1.7

R is Runoff, SI is Slope, LULC is Land use and Land cover, Li is Lithology, NDVI is Normalized Difference Vegetation Index, NDBI is Normalized Difference Built-up Index, MNDWI is Modified Normalized Difference Water Index, HSG is Hydrological Soil Group, DD is Drainage density, R/f is Rainfall, Dr is Distance from river, P is Permeability, TWI is Topographic Wetness Index, Pc is Profile curvature and Plc is Column total

**Table 6** Pairwise comparison matrix for FVI

Maps	Crop production	Road river interaction	Population density
Crop production	1.00	3.00	5.00
Road river interaction	0.33	1.00	3.00
Population density	0.20	0.33	1.00
Total	1.53	4.33	9.00

**Table 7** Normalized pairwise comparison matrix for FVI

Maps	Crop production	Road river interaction	Population density	Criteria weight
Crop production	0.65	0.69	0.56	63
Road river interaction	0.22	0.23	0.33	26
Population density	0.13	0.08	0.11	11

### 3.3.2 Slope map

In accordance with the AHP, the slope map was allocated a 16.4% weight. The resultant slope map was subsequently segregated into five discrete classifications according to the slope inclination measured in degrees. These categories are named Very Low, Low, Moderate, High and Very High. In the research region, the distribution of these categories accounts for approximately 65%, 21%, 7%, 5%, and 2% respectively. Figure 4 illustrates the slope map representing the characteristics of the research region.

### 3.3.3 LULC map

According to the AHP, the LULC map was assigned a 11.1% weight. The research area was classified into five primary classes: Forest, Barren, Agricultural, Water Bodies and Built-up. These categories make up approximately 25%, 10%, 55%, 4% and 6% of the research area, respectively. Figure 5 displays the LULC map representing the research region.

### 3.3.4 Lithology map

The AHP assigned a weight of 11.1% to the lithology map. The research region primarily comprises of four categories of rock structures: Granite, Quartz, Gneiss, and Laterite. These formations constitute approximately 1%, 17%, 54% and 28%, of the research region, respectively. Figure 6 displays the Lithology map, depicting the distribution and characteristics of various rock formations within the research region.

### 3.3.5 NDVI map

The AHP allocated a weight of 7.2% to the NDVI map. After generating the NDVI map, it was further divided into five groups based on the NDVI values. These groups are designated as Very Low, Low, Moderate, High, and Very High. Within the research region,

**Table 8** Weight and rank of all thematic maps for FHI

Thematic maps	% Influx (weight assigned)	Feature classes	Sub-class rank	Product (weight × rank)	CR
Runoff (mm)	16.4	29–38	1	16.4	0.04
		39–71	3	49.2	
		72–111	7	114.8	
		112–145	9	147.6	
Slope (%)	16.4	Very low	9	147.6	0.05
		Low	7	114.8	
		Moderate	5	82	
		High	3	49.2	
		Very high	1	16.4	
LULC	11.1	Water bodies	9	99.9	0.03
		Forest	1	11.1	
		Built-up	7	77.7	
		Agriculture	3	33.3	
		Barren	5	55.5	
Lithology	11.1	Gneiss	7	77.7	0.04
		Granite	9	99.9	
		Laterite	3	33.3	
		Quartz	5	55.5	
NDVI	7.2	Very high	1	7.2	0.02
		High	3	21.6	
		Moderate	5	36	
		Low	7	50.4	
NDBI	7.2	Very low	9	64.8	0.01
		Very high	1	7.2	
		High	3	21.6	
		Moderate	5	36	
		Low	7	50.4	
MNDWI	7.2	Very low	9	64.8	0.03
		Very low	1	7.2	
		Low	3	21.6	
		Moderate	5	36	
		High	7	50.4	
Hydrological soil group (HSG)	4.6	Very high	9	64.8	0.05
		HSG A	1	4.6	
		HSG B	3	13.8	
		HSG C	7	32.2	
Drainage density	4.6	HSG D	9	41.4	0.04
		Very low	9	41.4	
		Low	7	32.2	
		Medium	5	23	
		High	3	13.8	
		Very high	1	4.6	



**Table 8** (continued)

Thematic maps	% Influence (weight assigned)	Feature classes	Sub-class rank	Product (weight × rank)	CR
Rainfall (mm)	3.1	918–1043	1	3.1	0.02
		1044–1100	3	9.3	
		1101–1158	5	15.5	
		1159–1222	7	21.7	
		1223–1342	9	27.9	
Distance from river (m)	3.1	500	9	27.9	0.01
		1000	7	21.7	
		2000	5	15.5	
		3000	3	9.3	
		> 3000	1	3.1	
Permeability	2.3	Low	9	20.7	0.02
		Moderate	7	16.1	
		High	3	6.9	
		Very high	1	2.3	
TWI	2.3	Very low	1	2.3	0.04
		Low	3	6.9	
		Moderate	5	11.5	
		High	7	16.1	
		Very high	9	20.7	
Profile curvature	1.7	Low	1	1.7	0.03
		Moderate	5	8.5	
		High	9	15.3	
Plan curvature	1.7	Low	1	1.7	0.02
		Moderate	5	8.5	
		High	9	15.3	

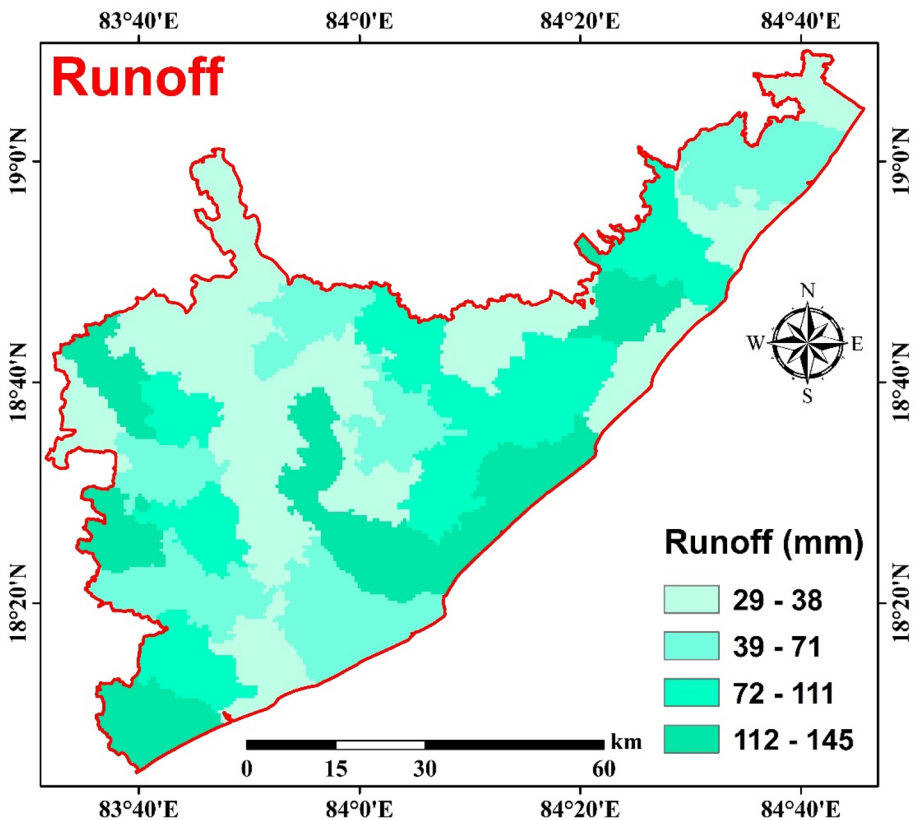
these categories represent approximately 17%, 33%, 28%, 19%, and 3% of the total area, respectively. Figure 7 visually represents the NDVI map, depicting the distribution and intensity of vegetation across the research region.

### 3.3.6 NDBI map

The AHP assigned a weight of 7.2% to the NDBI map. After generating the NDBI map, it was further divided into five distinct categories by considering the NDBI values. These distinct categories are designated as Very Low, Low, Moderate, High, and Very High. Within the research region, these categories represent approximately 14%, 19%, 23%, 26%, and 18% of the total research region, respectively. Figure 8 visually depicts the NDBI map, illustrating the spatial distribution and intensity of built-up areas across the research region.

**Table 9** Weight and rank of all thematic maps for FVI

Thematic maps	% Influence (weight assigned)	Feature classes	Sub-class rank	CR
Crop production (Kg/Ha)	63	2389–3089	1	0.03
		3090–3970	3	
		3971–4952	5	
		4953–5808	7	
		5809–6403	9	
Population density (persons per km <sup>2</sup> )	26	214–515	1	0.04
		515.1–653	3	
		653.1–797	5	
		797.1–1064	7	
		1064.1–1276	9	
Road river intersection (no. of points per km <sup>2</sup> )	11	0–2	1	0.01
		3–5	3	
		6–8	7	
		9–11	9	

**Fig. 3** Runoff map of the study area

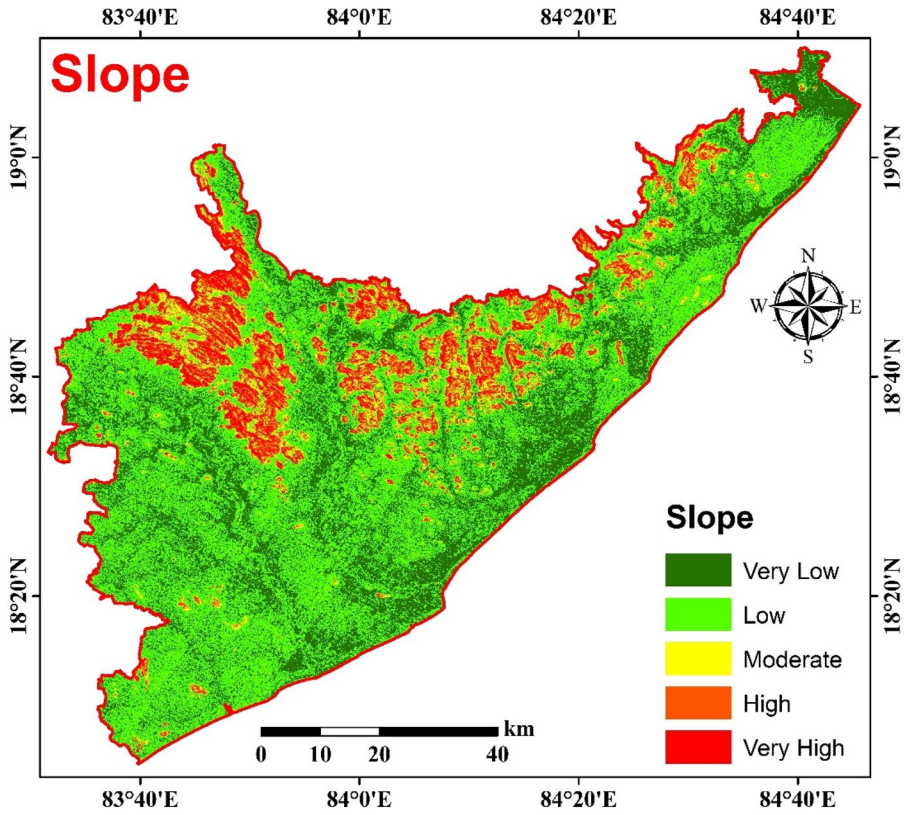


Fig. 4 Slope map of the study area

### 3.3.7 MNDWI map

The AHP allocated a weight of 7.2% to the MNDWI map. Upon generating the MNDWI (Modified Normalized Difference Water Index) map, it underwent classification into five distinct categories based on the MNDWI values. These groups were labeled as Very Low, Low, Moderate, High, and Very High, representing approximately 21%, 38%, 33%, 5%, and 3% of the total research region, respectively. The MNDWI map is visually depicted in the Fig. 9.

### 3.3.8 HSG map

According to the AHP, the HSG (Hydrologic Soil Group) map was assigned a weight of 4.6%. In the research region, the dominant soil groups consist of four groups: A, B, C, and D, covering approximately 17%, 21%, 29%, and 33% of the total research region, respectively. The HSG map for the research region, showcasing the spatial representation and distribution of different HSG categories is illustrated in Fig. 10.

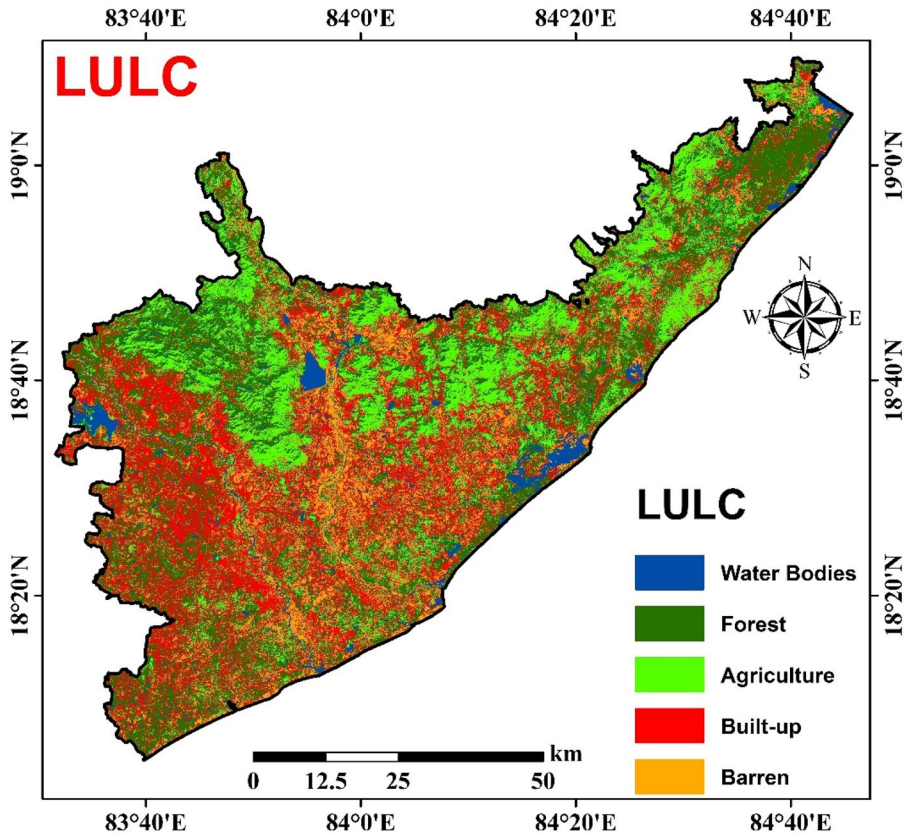


Fig. 5 LULC map of the study area

### 3.3.9 DD map

The AHP assigned a weight of 4.6% to the DD map. The DD map displays the concentration of drainage in the research area and is sorted into five classifications: very Low, Low, Moderate, High, and very High. These groups represent approximately 19%, 24%, 27%, 20%, 7%, and 10% of the total research region, respectively. The DD map of the research region is shown in the Fig. 11.

### 3.3.10 Rainfall map

The AHP assigned a weight of 3.1% to the Rainfall map. The rainfall map was classified into five distinct groups based on rainfall ranges, namely 918–1043 mm, 1044–1100 mm, 1101–1158 mm, 1159–1222 mm, and 1223–1342 mm. These categories represent approximately 13%, 40%, 25%, 18%, and 3% of the total research region, respectively. For a visual representation of the rainfall distribution, refer to Fig. 12.

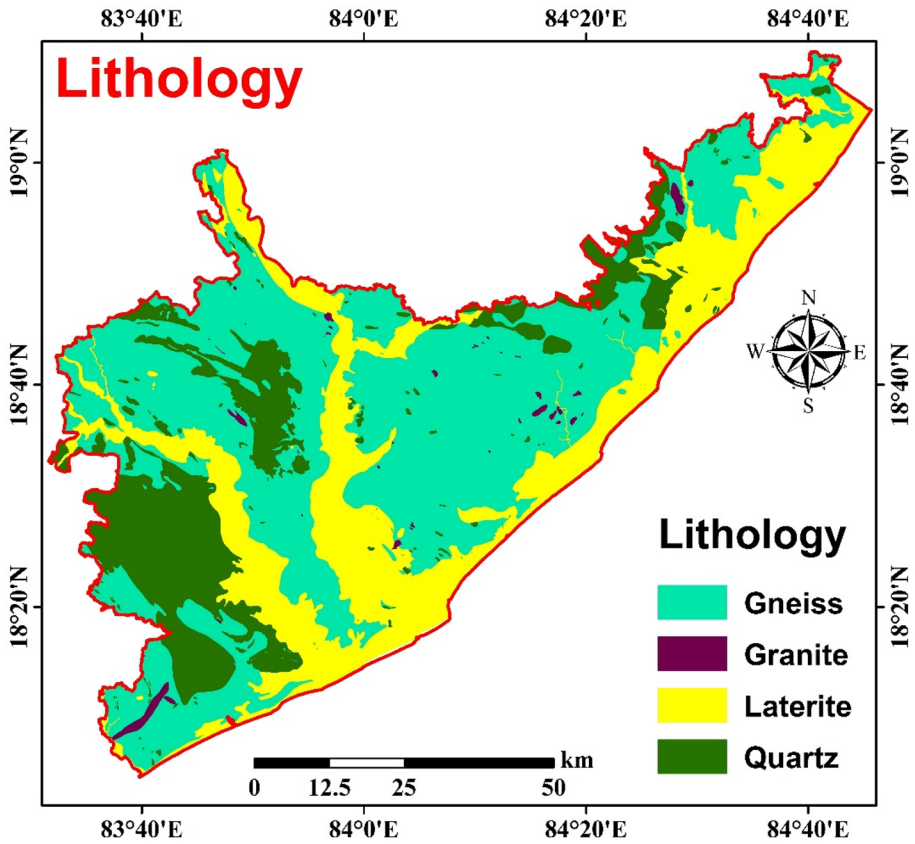


Fig. 6 Lithology map of the study area

### 3.3.11 Distance from river map

The AHP allocated a weight of 3.1% to the Distance from River map. The research region was divided into six distinct groups: 500 m, 1000 m, 2000 m, 3000 m, and distances greater than 3000 m. These categories represent approximately 6%, 11%, 19%, 26%, and 39% of the total research region, respectively. Distance from river map is shown in the Fig. 13.

### 3.3.12 Permeability map

The AHP assigned a weight of 2.3% to the Permeability map. The Permeability map is divided into four categories: Low, Moderate, High, and Very High. These groups represent approximately 17%, 21%, 29%, 7%, and 33% of the total research region, respectively. The permeability map of the research region is shown in the Fig. 14.

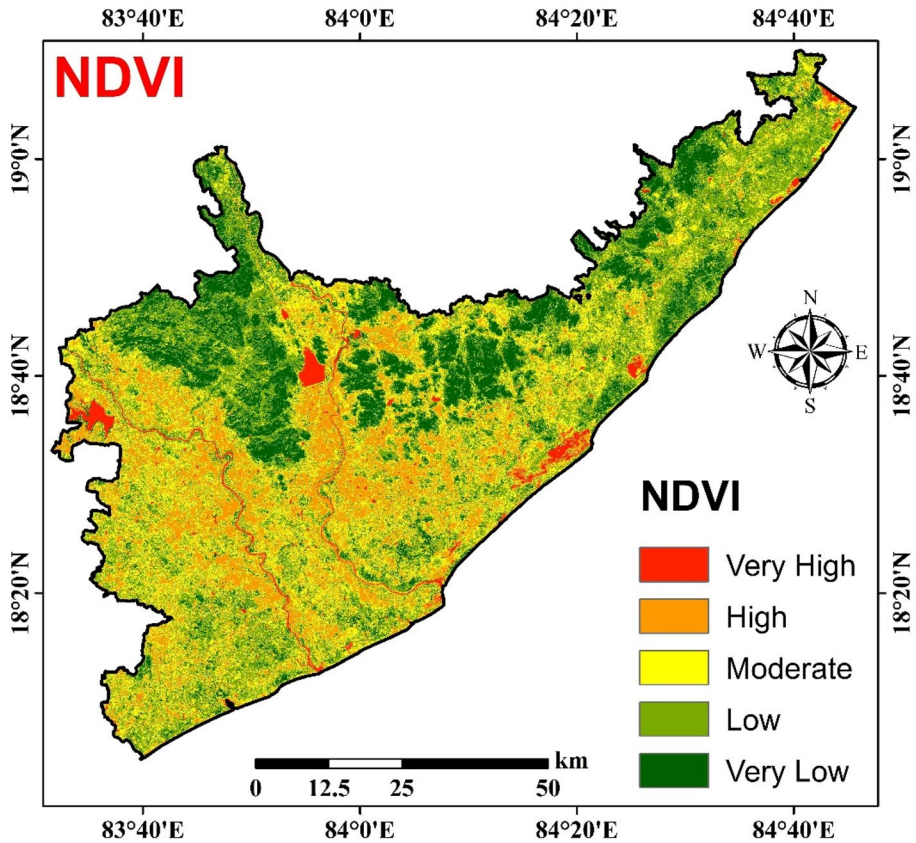


Fig. 7 NDVI map of the study area

### 3.3.13 TWI map

The AHP assigned a weight of 2.3% to the TWI map. The TWI map of the research area was divided into five categories: Very Low, Low, Moderate, High, and Very High, accounting for 23%, 42%, 15%, 17%, and 3% of the research region, respectively. Figure 15 displays the TWI map of the research region.

### 3.3.14 Profile and plan curvature map

The weights assigned to both the plan and profile curvature maps were 1.7% each, based on the AHP. The profile curvature map was classified into three categories: low, moderate and high, representing 10%, 69%, and 21% of the research region, respectively. The plan curvature map was classified into three categories: low, moderate and high, representing 9%, 73%, and 18% of the research region, respectively. Figures 16 and 17 displays the profile and plan curvature map of the study area, respectively.

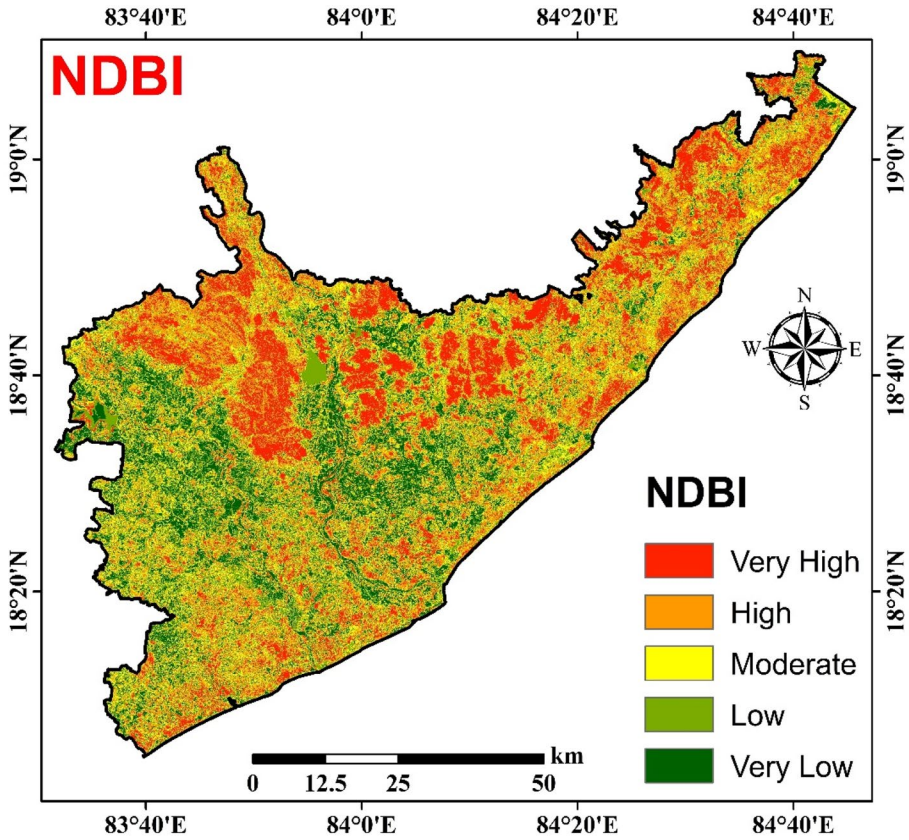


Fig. 8 NDBI map of the study area

### 3.4 FHI

The FHI map for the research region was developed in ArcGIS software by overlaying several thematic maps, including Runoff, Slope, LULC, Lithology, NDVI, NDBI, MNDWI, HSG, DD, Rainfall, Distance from River, Permeability, TWI, Profile, and Plan Curvature. The weights and ranks assigned to each of these 15 thematic maps and their sub-classes, using AHP methodology, were considered during the overlay process. The weighted overlay method in ArcGIS was employed for this purpose. By applying the weighted overlay method and considering the assigned weights and ranks, the FHI map was generated. This map serves as a comprehensive representation of flood hazard potential in the research region, incorporating multiple factors and their respective influences on flood occurrence.

According to the analysis of the FHI map, the research area was categorized into five separate regions: very high, high, medium, low, and very low FHI. These zones accounted for 41%, 25%, 24%, 8%, and 2% of the research region, respectively. The FHI map, shown in Fig. 18, was created by incorporating information from all 15 thematic maps.

From the analysis of Fig. 18, it was evident that 66% of the region fell into the high and very high FHI classifications. This can be attributed to favorable factors such as low and very low runoff, gentle slopes, presence of water bodies and built-up areas in the LULC

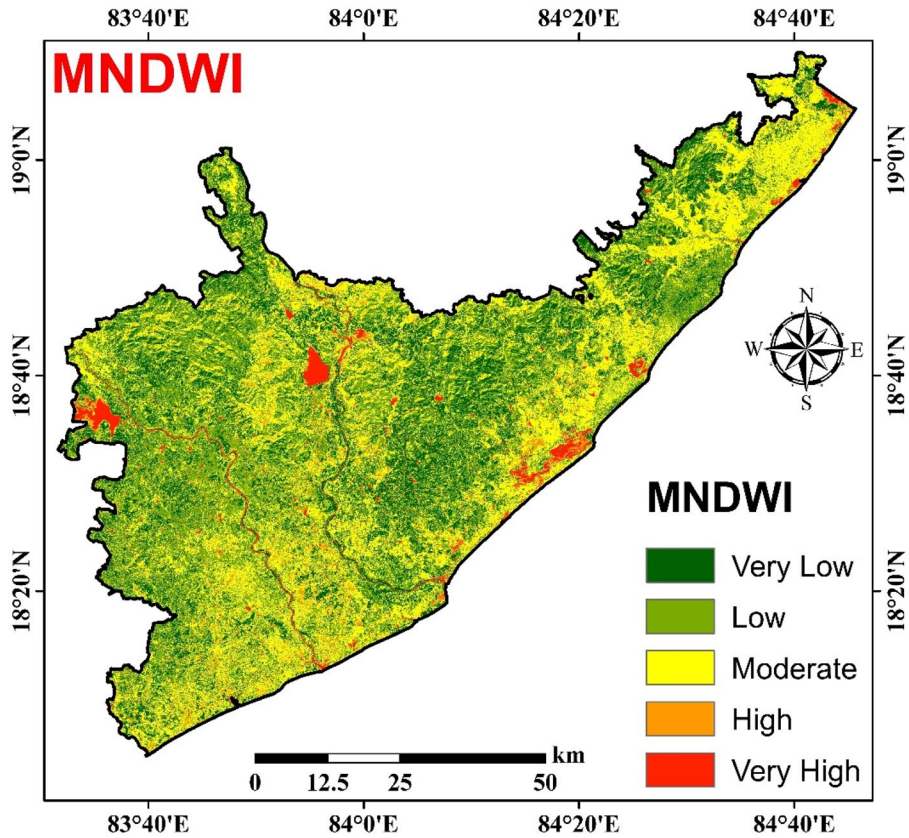


Fig. 9 MNDWI map of the study area

data, and the predominant lithology of granite and gneiss in the Srikakulam district of Andhra Pradesh, India, where the research was conducted. However, 34% of the region was classified as low and moderate FHI zones. This can be attributed to unfavorable factors such as presence of mountains, steep or high slopes, low runoff, and the presence of forests and agricultural land.

### 3.5 Sensitivity analysis of FHI

Table 10 displays the results of the map removal sensitivity analysis, while Table 11 presents the outcomes of the single parameter sensitivity analysis. Based on Table 10, it is evident that the runoff and slope maps have the most significant impact on the FHI, followed by the LULC, lithology, NDVI, NDBI, and MNDWI maps, which have a moderate impact. Conversely, the Curvature and TWI maps exhibit the lowest impact on FHI computation. The elimination of the runoff and slope maps results in substantial variations as indicated by high values of the variation index. This signifies that runoff and slope shows a vital role in developing the FHI for the research region.

Table 11 provides the percentage of effective weights for all thematic maps. The results demonstrate that higher empirical weights correspond to higher effective



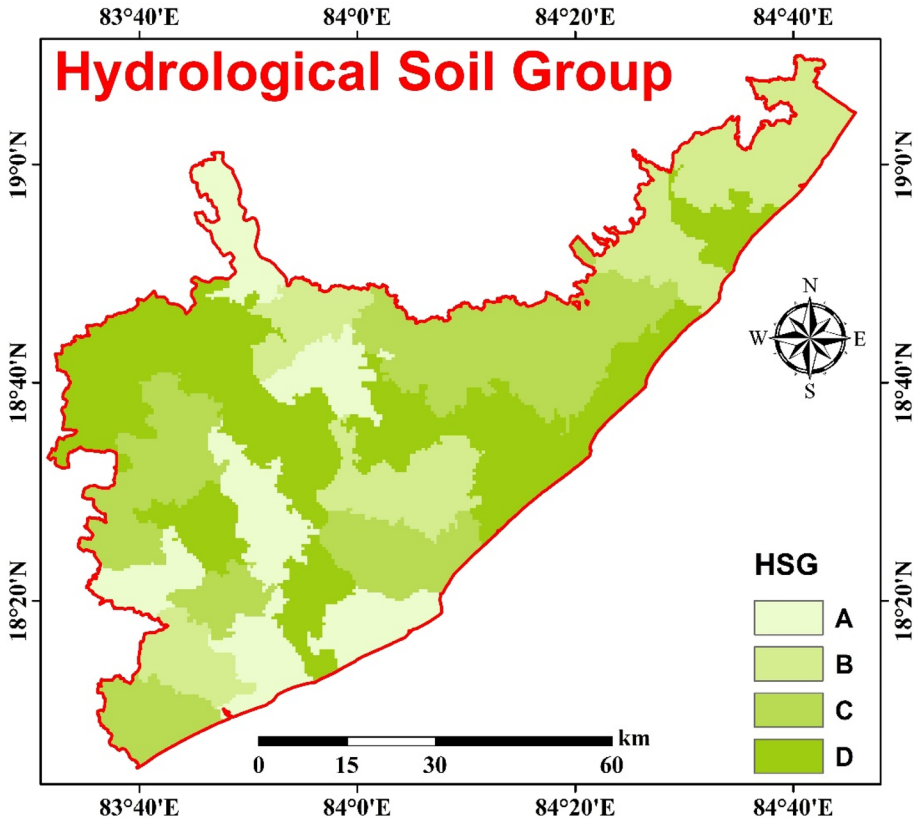


Fig. 10 HSG map of the study area

weights, implying their greater influence on the FHI calculation. Table 12 illustrates the changes in the percentage of areas within different FHI categories (i.e., very high, high, moderate, low, and very low) after the removal of individual thematic maps. The outcomes indicate that excluding the runoff map and slope map significantly impact the FHI by increasing the area classified as low suitability by 35.3% and 27.6%, respectively. However, the exclusion of the TWI and Curvature maps exhibits a minor influence on the FHI.

### 3.6 Development of FVI

#### 3.6.1 Crop production map

The crop production map was allocated a weight of 63% based on the AHP. Using ArcGIS software, a Crop Production Map was created, classifying the tehsil-wise total yield into five categories: 2389–3089, 3090–3970, 3971–4952, 4953–5808 and 5809–6403 kg per ha. These categories represent 4%, 13%, 17%, 25%, 30% and 28% of the research region, respectively. Figure 19 showcases the Crop Production Map of the research region.

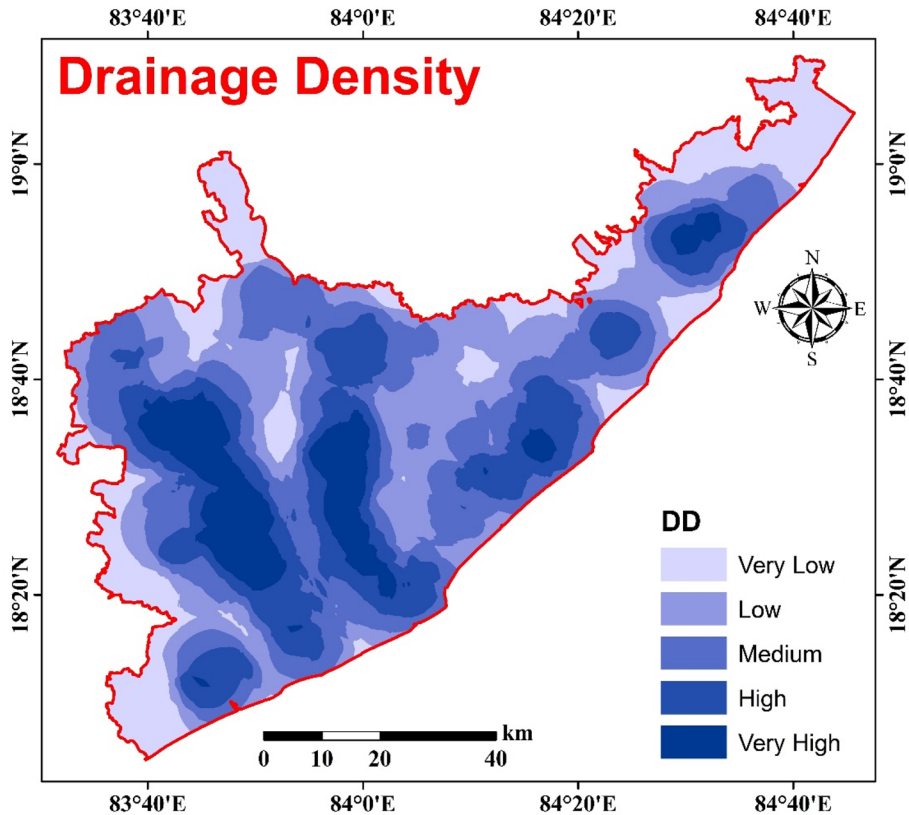


Fig. 11 DD map of the study area

### 3.6.2 Population density map

The population density map was given a weight of 26% based on the AHP. The population density map was classified into five categories: 214–515, 515.1–653, 653.1–797, 797.1–1064 and 1064.1–1276 persons per sq. km., representing 14%, 24%, 17%, 36% and 10% of the research region, respectively. The population density map of the research region is shown in Fig. 20.

### 3.6.3 Road river intersection map

The road river intersection map was given a weight of 11% based on the AHP. The map depicting road-river interactions was divided into four categories: 0–2, 3–5, 6–8 and 9–11 points per sq. km. These categories represent 68%, 24%, 7% and 1% of the research region, respectively. Figure 21 showcases the road-river interaction map of the research region, offering a visual representation of these categories.

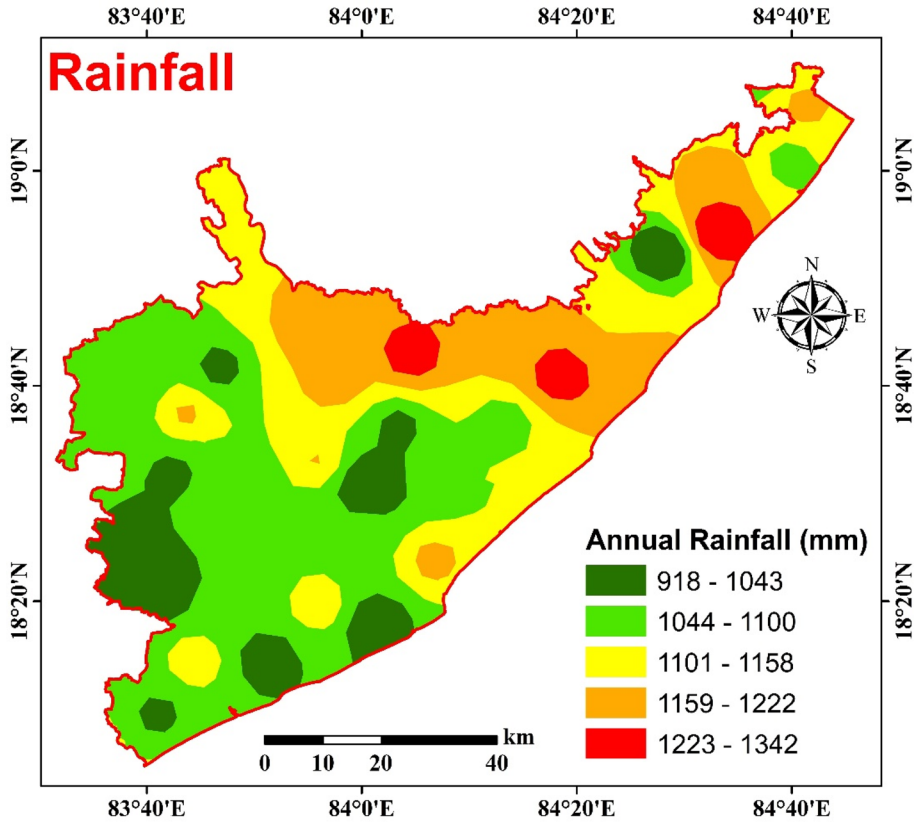


Fig. 12 Rainfall map of the study area

### 3.7 FVI

The FVI map for the research region was generated using ArcGIS software by overlaying three thematic maps: population density, road river intersection and crop production. The ranks and weights allocated to all of these maps and their sub-categories, based on the AHP, were considered during the overlay process. The weighted overlay method in ArcGIS was employed for this purpose. The production of the FVI map was achieved through the utilization of the weighted overlay technique, which involved the integration of the designated weights and ranking. This map provides a comprehensive representation of flood vulnerability in the research region, taking into account the influences of population density, crop production, and road river interaction.

According to the FVI map analysis, the research region has been classified into five distinct regions: very high, high, moderate, low, and very low FVI. These regions account for 20%, 22%, 29%, 13%, and 16% of the research region, respectively. The FVI map, shown in Fig. 22, was created by incorporating information from all three thematic maps.

From the analysis of Fig. 22, it is evident that 42% of the area falls into the very high and high FVI categories. This can be attributed to favorable conditions such as higher crop production, high population density, and a significant number of road river intersections in

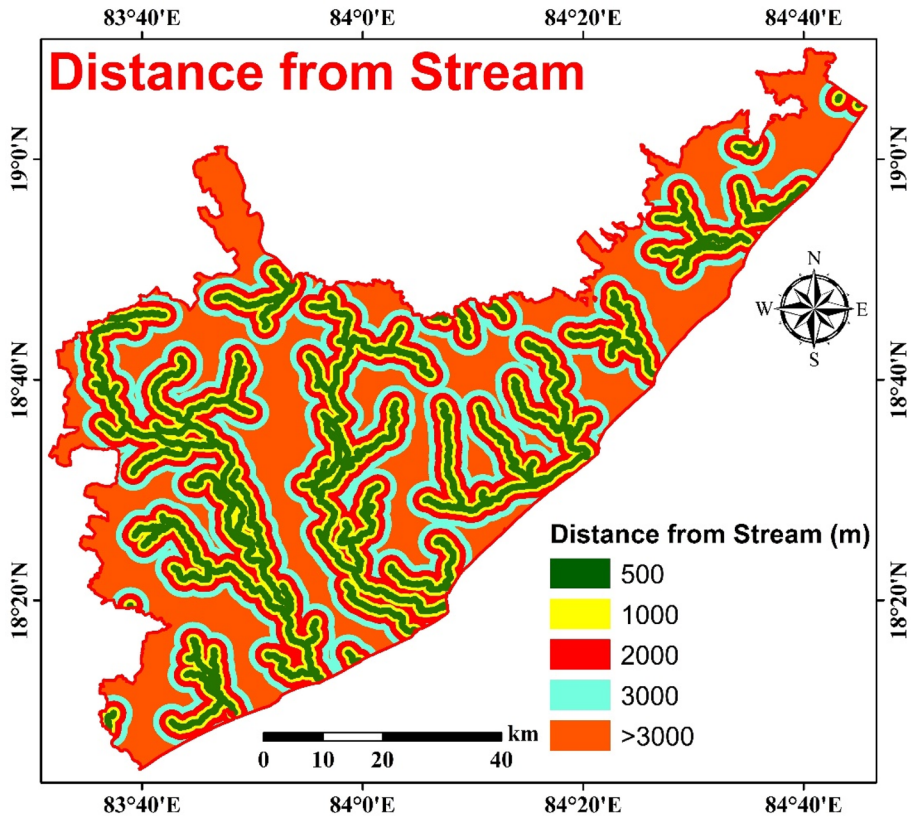


Fig. 13 Distance from river map of the study area

the research area. However, 58% of the area is categorized as moderate and low FVI zones. This can be attributed to unfavorable conditions such as lower crop production, lower population density, and a lower density of road river intersections.

### 3.8 Sensitivity analysis of FVI

Table 13 presents the results of the map removal sensitivity analysis, while Table 14 displays the outcomes of the single parameter sensitivity analysis. Based on Table 13, it is evident that the crop production map has the greatest impact on the FVI, followed by the population density map, while the road river intersection map has the lowest impact on FVI computation. The results of the variation index indicate that the exclusion of the crop production map results in significant variations, followed by the elimination of the population density map. This indicates that the crop production map has a substantial impact on the FVI for the research region. Table 14 provides the effective weights of all thematic maps expressed as percentages. The results demonstrate that higher empirical weights correspond to higher effective weights, indicating their greater influence on the FVI calculation.

Table 15 illustrates the changes in the area percentage within different FVI categories (i.e., very high, high, moderate, low, and very low) after the removal of individual thematic

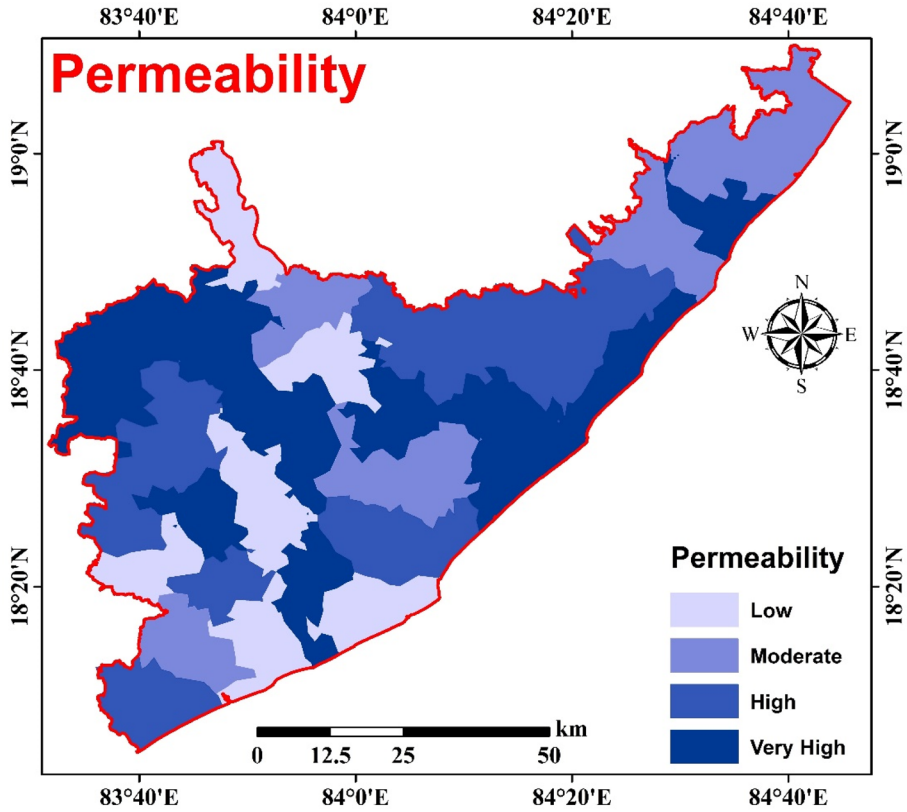


Fig. 14 Permeability map of the study area

maps. The outcomes indicate that excluding the crop production map significantly impacts the FVI by increasing the area classified as low FVI by 41.3%. However, the exclusion of the road river intersection map exhibits a lesser impact on the FVI.

### 3.9 Development of FRI

To generate a comprehensive FRI map for the research region, a combination of FHI and FVI maps was employed. By leveraging the power of the weighted sum method in ArcGIS software, these maps were integrated together to develop the final result. Figure 23 provides an overview of the FRI map for the research region. The FRI map was divided into five divisions: high-risk, high, moderate, low, and very low zones, encompassing 28%, 20%, 16%, 28%, and 8% of the research region, respectively. Notably, 48% of the research region falls within the very high-risk and high-risk zones, indicating favorable conditions such as high runoff, flat slopes, the presence of water bodies and built-up areas, high rainfall, and dense crop production and population. Conversely, 36% of the research region is categorized as low and very low risk, attributed to factors like low runoff, steep slopes, the presence of forests and agricultural land, low rainfall, and lower crop production and population density.

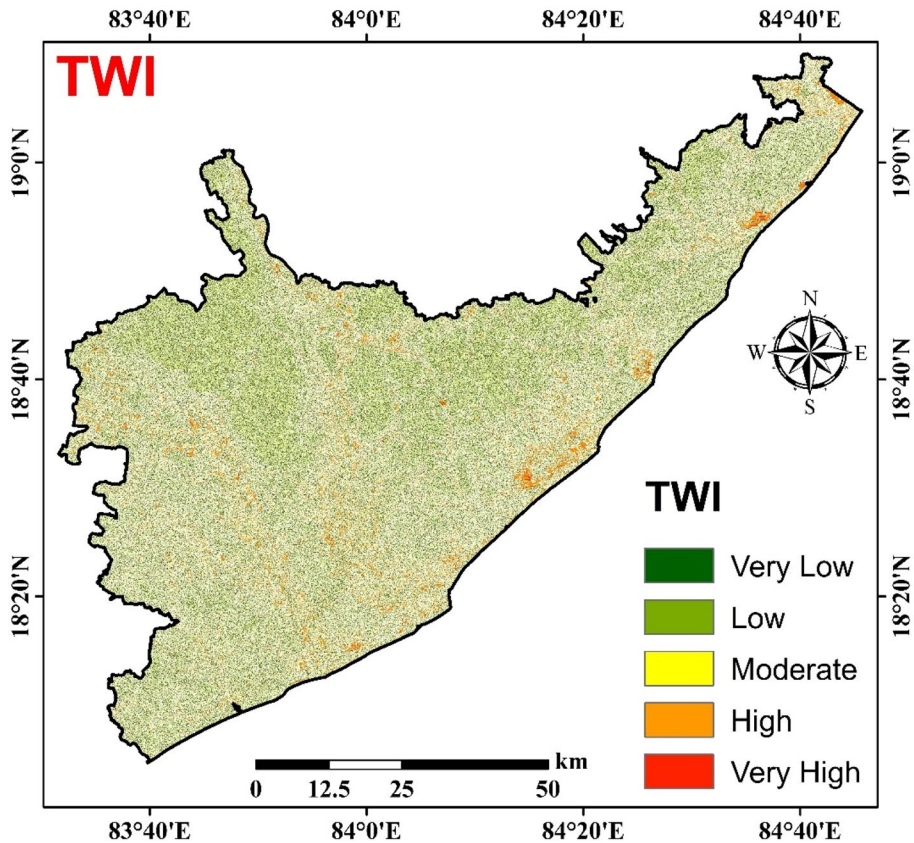


Fig. 15 TWI map of the study area

In Table 16, the village and area mapping based on the FRI classification is presented, providing a detailed understanding of the risk distribution across the research region. Furthermore, Fig. 24 depicts a histogram comparison of the FHI, FVI and FRI percentages for different categories within the research region.

These findings contribute to a comprehensive understanding of the flood risk landscape, aiding in the formulation of appropriate mitigation and disaster management strategies. By identifying areas with high vulnerability and risk, decision-makers can focus resources and interventions where they are most needed, ensuring the safety and well-being of the population and minimizing potential damage caused by flooding events.

### 3.10 Validation of FRI map

A critical procedure called "model validation" entails methodically contrasting a model's outputs with unbiased real-world data. Assessing the level of concordance between the recorded data or real conditions and the quantitative and qualitative outcomes of the model is the aim. Scholars often use a variety of models to evaluate flood risk in various parts of the world. To make sure the model's outputs appropriately reflect the circumstances in the actual world, it is crucial to validate them.

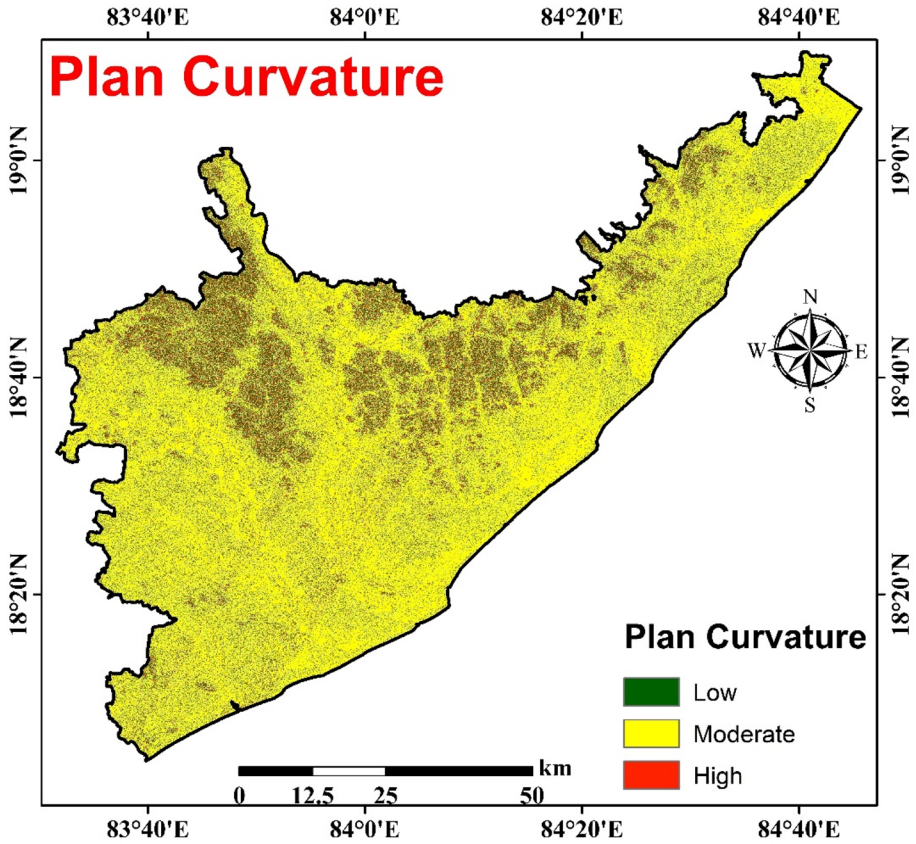


Fig. 16 Plan Curvature map of the study area

To validate the FRI map, a total of 50 points were carefully selected, with 10 points allocated to each category. The validation process involved utilizing the ROC analysis. In the ROC curve, the x-axis illustrates the False Positive Rate (FPR), which quantifies how frequently the classifier erroneously classifies negative instances as positive. Meanwhile, the y-axis represents the True Positive Rate (TPR), also known as sensitivity, which assesses the model's proficiency in accurately identifying positive instances. To verify the accuracy of the ground truth points, field visits were conducted, and data regarding flooding zones (based on previous flooding records) were collected from the Andhra Pradesh State Disaster Management Authority (APSDMA) in Andhra Pradesh, India. Among the 50 points, only 3 points exhibited discrepancies compared to the FRI map prepared using ArcGIS software. These ground truth points, along with the FRI map, were visually represented in Fig. 25. In Fig. 25, the ground truth points were represented by different shapes whereas different color indicates classified classes of FRI using ArcGIS. To validate the FRI map, a comparison between the ground truth points and the produced FRI map was performed with the use of SPSS software. The validation process included cross-validation using the ROC curve, as depicted in Fig. 26. The Area Under the Curve (AUC) statistic, which determines the effectiveness of a variable in distinguishing between two groups, were calculated. The AUC in a ROC curve is a measure of the overall performance of a

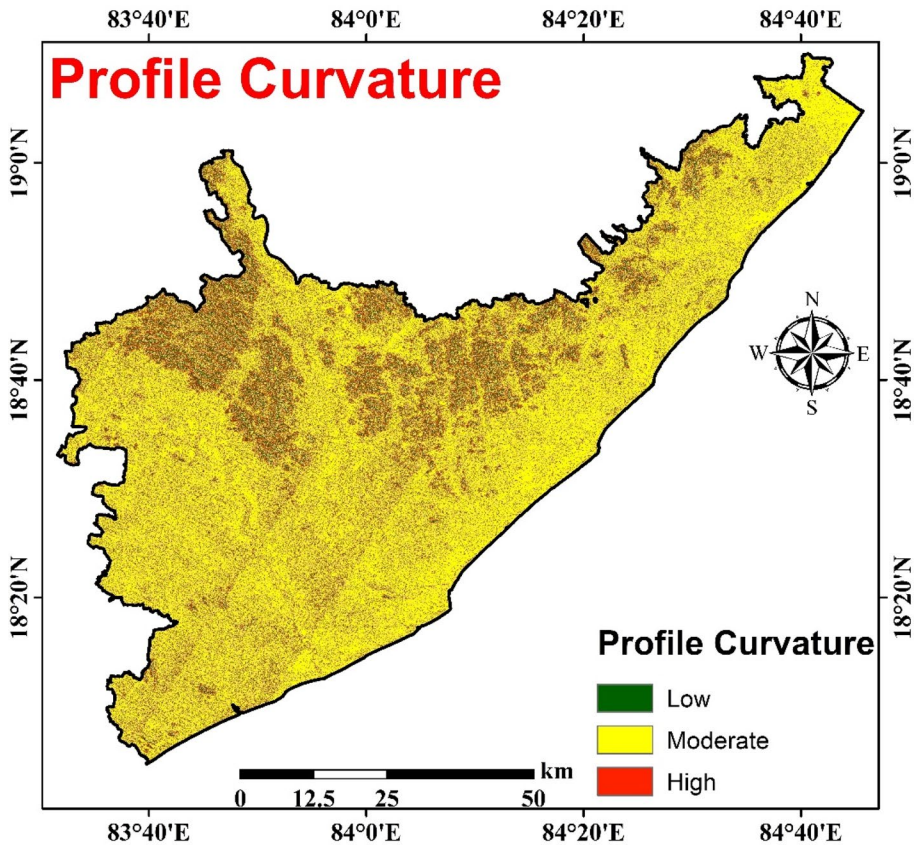


Fig. 17 Profile Curvature map of the study area

classification model. It quantifies the model's ability to distinguish between positive and negative cases. A higher AUC indicates better performance, with 1 being perfect. An AUC of 0.5 suggests a model that performs no better than random guessing, while values above 0.5 show some level of discrimination. The closer the AUC is to 1, the better the model's ability to correctly classify positive cases while minimizing false positives. In case of FRI map, the AUC value was found to be 0.89, indicating that the AHP approach employed in the model resulted in highly accurate predictions.

#### 4 Discussion and conclusions

The research region under investigation experiences frequent flood and drought situations, both during the monsoon and non-monsoon seasons. These occurrences are primarily caused by factors such as heavy rainfall, high runoff, flat slopes, low infiltration, low permeability, and a lack of proper flood management systems (Desalegn & Mulu, 2020; Gazi et al., 2019). In this study, the aim was to identify FRI zones using a combination of the AHP, GIS approach, and remote sensing techniques. The identification of high-risk locations within the FRI zones was of utmost importance to establish effective



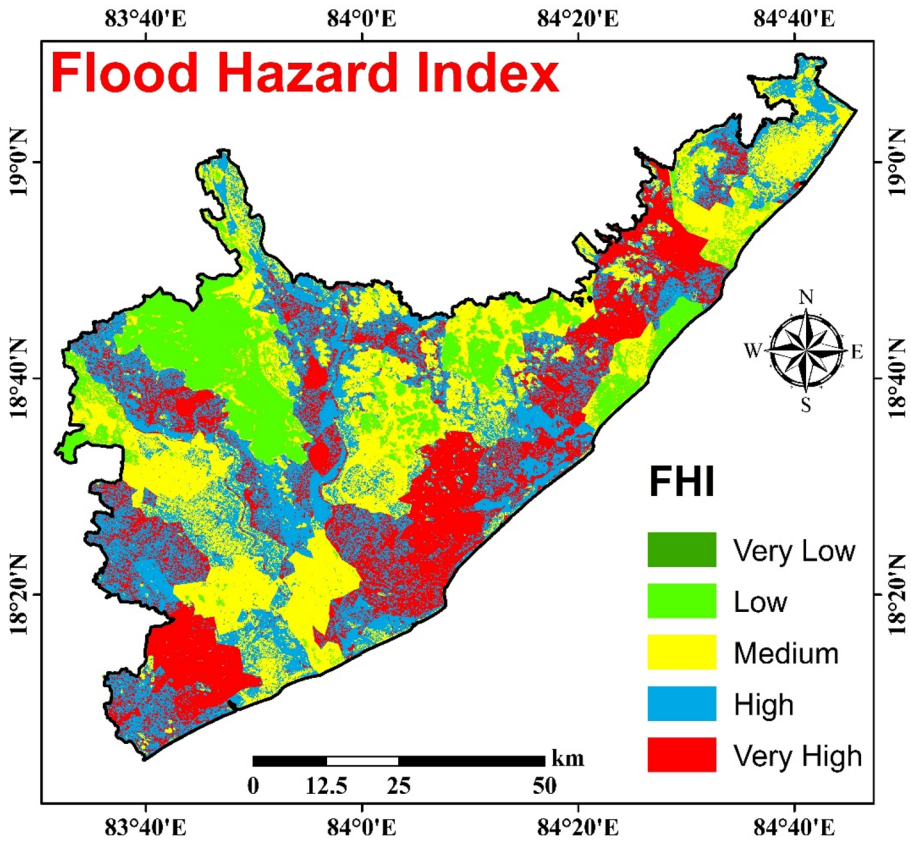


Fig. 18 FHI map of the study area

**Table 10** Statistical analysis of map removal sensitivity analysis for FHI

Thematic map removed	Variation Index (%)			
	Min	Max	Mean	SD
Runoff	0.42	6.32	4.01	0.89
Slope	0.28	6.20	3.95	0.85
LULC	0.29	6.11	3.51	0.76
Lithology	0.33	5.76	3.69	0.67
NDVI	0.42	5.63	3.61	0.58
NDBI	0.63	5.14	3.25	0.54
MNDWI	0.58	5.02	3.03	0.47
HSG	0.75	4.63	2.69	0.46
DD	0.83	4.22	2.86	0.41
Rain fall	0.33	4.35	2.31	0.32
Distance from river	0.21	3.78	2.08	0.31
Permeability	0.79	3.54	1.68	0.29
TWI	0.29	3.46	1.32	0.26
Plan curvature	0.43	3.12	1.03	0.25
Profile curvature	0.37	3.29	1.26	0.24

**Table 11** Statistical analysis of single parameter sensitivity analysis for FHI

Thematic maps	Empirical weight (%)	Effective weight (%)			
		Min	Max	Mean	SD
Runoff	16.4	6.3	61.3	23.2	11.3
Slope	16.4	6.3	61.3	23.2	11.3
LULC	11.1	4.9	43.8	14.9	8.6
Lithology	11.1	4.9	43.8	14.9	8.6
NDVI	7.2	3.7	24.2	9.6	4.3
NDBI	7.2	3.7	24.2	9.6	4.3
MNDWI	7.2	3.7	24.2	9.6	4.3
HSG	4.6	2.6	13.5	6.2	2.8
DD	4.6	2.6	13.5	6.2	2.8
Rain fall	3.1	1.8	8.3	4.1	1.6
Distance from river	3.1	1.8	8.3	4.1	1.6
Permeability	2.3	1.2	5.1	2.3	1.1
TWI	2.3	1.2	5.1	2.3	1.1
Plan curvature	1.7	0.8	3.6	1.7	0.7
Profile curvature	1.7	0.8	3.6	1.7	0.7

**Table 12** Changes of the FHI with removal of the thematic map

Thematic maps	FHI (%)				
	Very low	Low	Moderate	High	Very high
Runoff	+35.3	+38.3	-31.2	-17.6	-7.2
Slope	+27.6	+29.1	+21.5	-12.8	-5.1
LULC	+19.3	+20.5	-14.6	-9.2	-3.3
Lithology	+12.2	+13.7	-9.6	-5.8	-2.3
NDVI	+7.3	+8.1	-7.1	-3.1	-0.8
NDBI	+7.8	+8.9	-12.3	-9.6	-2.3
MNDWI	+7.1	-7.6	+7.3	+3.2	-1.8
HSG	+5.2	+3.4	-2.9	-0.7	+2.3
DD	-3.5	+12.6	-8.2	-6.3	-2.8
Rain fall	-2.8	+1.8	+1.6	-0.6	-1.7
Distance from river	-1.8	-1.3	+2.2	+2.1	+3.1
Permeability	+2.4	+3.5	-2.3	-1.4	-0.9
TWI	+1.2	+1.6	-3.1	-1.5	-0.7
Plan Curvature	+1.3	+1.3	-3.3	-1.8	-1.3
Profile Curvature	+1.1	-1.4	+2.6	+1.7	-1.6

'+' indicates increase in area and '-' indicates decrease in area

flood management systems (Velasco et al., 2016). The implementation of such systems would help minimize losses resulting from floods, improve water storage facilities in the research region to meet domestic, irrigation, and industrial needs during non-monsoon

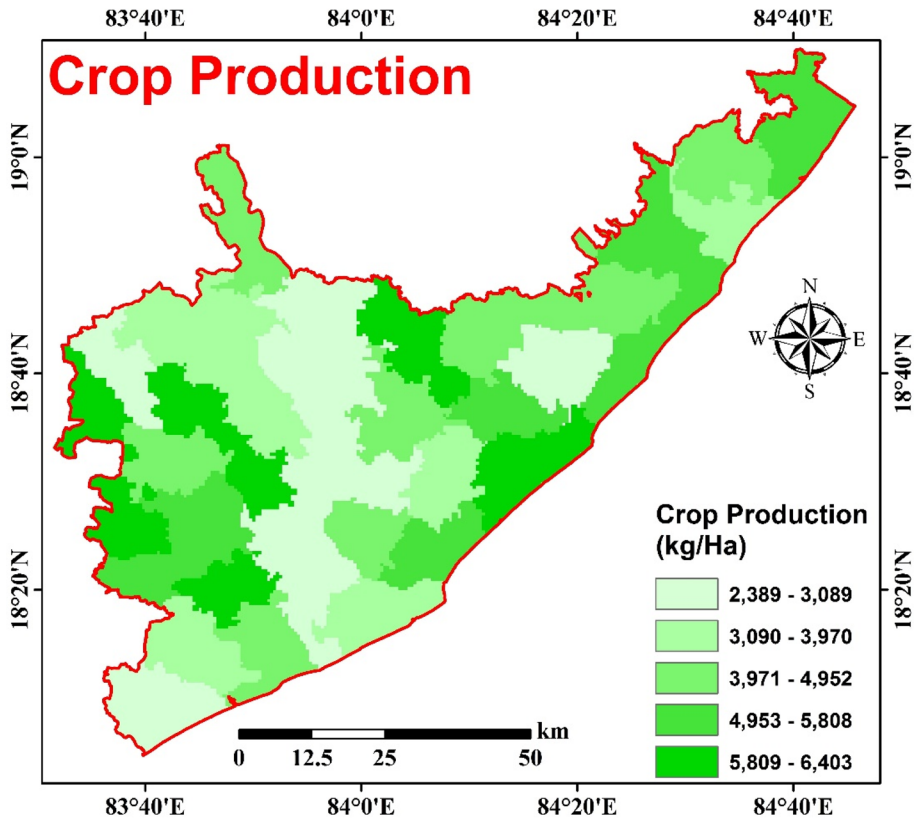


Fig. 19 CP map of the study area

periods, and reduce the adverse environmental impacts caused by droughts (Yang et al., 2018; Abu El-Magd et al., 2020; Gandini et al., 2020). Several existing procedures were considered during the study; however, many of them proved inadequate for specific zones due to regional conditions, time constraints, social factors, or political challenges (Arrighi, 2021; Baquedano & Ferreira, 2021; Chen et al., 2018; Doorga et al., 2022; Memon et al., 2020; Merz et al., 2021; Petroselli et al., 2019; Requena et al., 2018). By incorporating GIS and remote sensing technologies, along with methods to address multicollinearity and the AHP technique, the accuracy of the output was significantly improved (Arya & Singh, 2021; Chakraborty & Mukhopadhyay, 2019; Martinez-Gomariz et al., 2021; Ray, 2023). Additionally, this integrated approach saved a considerable amount of time in the analysis process (Amare & Okubay, 2019; Samela et al., 2018).

In previous attempts to develop the FRI map, a maximum of 10 to 12 thematic maps were utilized. However, the final accuracy of these maps ranged between 0.73 and 0.77 as shown in Table 1. It is important to note that these accuracies were achieved without considering the factors of multicollinearity check and sensitivity analysis as shown in Table 1. To enhance the accuracy of the FRI map, the current study incorporated

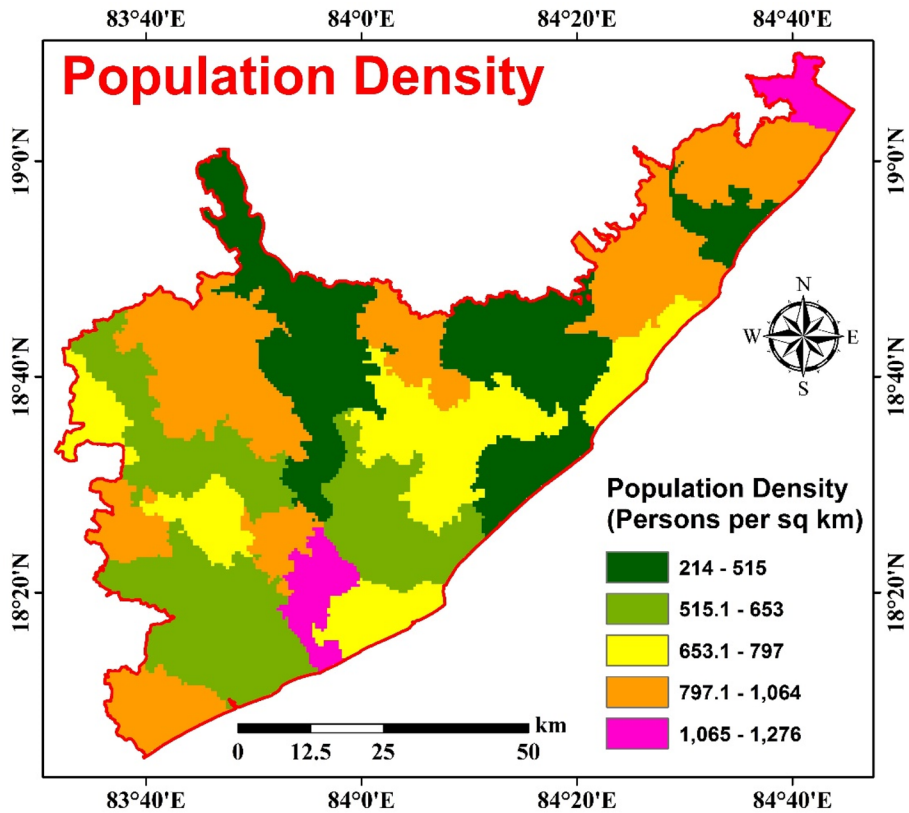


Fig. 20 PD map of the study area

additional steps such as multicollinearity check and sensitivity analysis. By including these measures, the accuracy of the thematic map was significantly improved, reaching a value of 0.89. This indicates a substantial enhancement in the accuracy and reliability of the FRI map compared to previous attempts (Dayala et al., 2020; Ferreira & Santos, 2020; Hussain et al., 2021; Mundhe, 2019; Requena et al., 2018; Samela et al., 2018; Vojtek & Vojtekova, 2019). The multicollinearity check helps identify and address the issue of collinear relationships between predictor input thematic maps, ensuring that they are not redundantly contributing to the model. By eliminating multicollinearity, the FRI map becomes more robust and reliable in capturing the true flood risk patterns in the research region. Additionally, sensitivity analysis allows for a comprehensive evaluation of the model's performance by examining the impact of varying input thematic maps. This analysis ensures that the FRI map's outputs are not overly sensitive to specific input thematic maps, strengthening its credibility and accuracy (Ray, 2023).

The present study introduced a novel approach by incorporating multicollinearity checks and sensitivity analysis into the development of the FRI map. Unlike previous attempts that used a limited number of thematic maps as shown in Table 1, this study

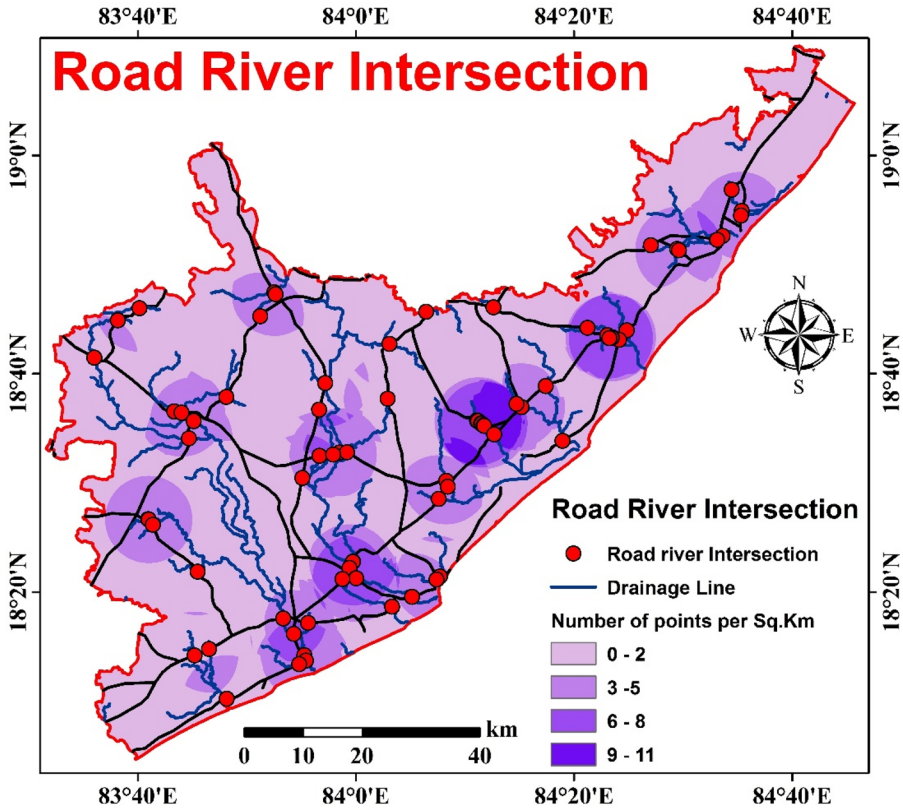


Fig. 21 RRI map of the study area

considered a total of 18 thematic maps for delineating the FRI map. The inclusion of multicollinearity checks was found to be crucial in identifying high-risk zones. By addressing multicollinearity, the study minimized uncertainty within the data, thereby enhancing the accuracy of the FRI map’s outcomes. This step helped ensure that the identified high-risk zones were based on solid and independent information, improving the reliability of the results (Ray, 2023).

Additionally, sensitivity analysis played a significant role in the study. The AHP was utilized to evaluate the importance of various thematic maps relative to one another, thereby confirming the accuracy of the assigned weights for each thematic map (Amare & Okubay, 2019; Bonazza et al., 2018; Xiao et al., 2021). By conducting sensitivity analysis, the study was able to ascertain the relative significance and contribution of each thematic map to the overall FRI map. This analysis provided valuable insights into the relative influence of different variables and helped validate the weighting scheme derived from the AHP process (Prieto et al., 2020; Ray, 2023; Singh et al., 2020; Teng et al., 2017).

In summary, the inclusion of multicollinearity checks and sensitivity analysis in the study brought several benefits. Multicollinearity checks increased the accuracy of the FRI

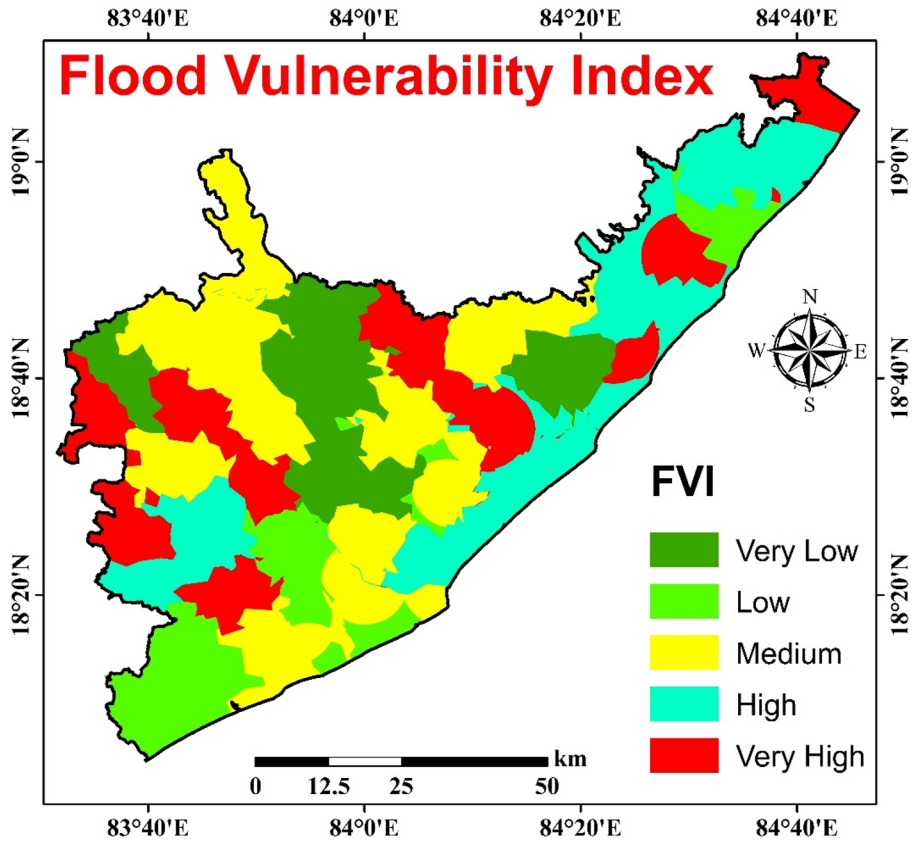


Fig. 22 FVI map of the study area

**Table 13** Statistical analysis of map removal sensitivity analysis for FVI

Thematic map removed	Variation index (%)			
	Min	Max	Mean	SD
Crop production	0.53	7.68	5.21	0.93
Road river interaction	0.34	6.12	3.83	0.81
Population density	0.29	5.23	3.33	0.72

**Table 14** Statistical analysis of single parameter sensitivity analysis for FVI

Thematic maps	Empirical weight (%)	Effective weight (%)			
		Min	Max	Mean	SD
Crop Production	63	7.3	68.3	25.1	13.2
Road River Interaction	26	5.8	41.2	14.6	8.3
Population Density	11	3.5	26.1	9.1	5.4

**Table 15** Changes of the FVI with removal of the thematic map

Thematic maps	FVI (%)				
	Very low	Low	Moderate	High	Very high
Crop production	+ 41.3	+ 36.7	- 33.8	- 18.4	- 8.6
Road river interaction	+ 21.3	+ 26.8	+ 18.5	- 14.6	- 4.3
Population density	+ 15.7	+ 18.3	- 13.1	- 7.7	- 2.2

‘+’ indicates increase in area and ‘-’ indicates decrease in area

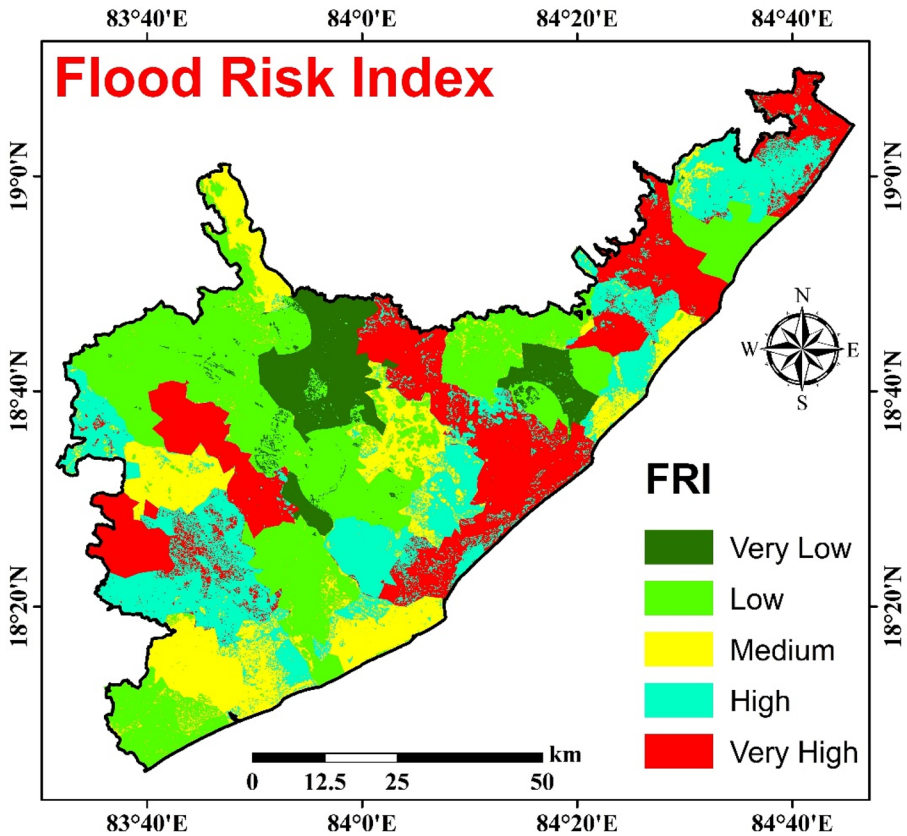


**Fig. 23** FRI map of the study area

map by reducing uncertainty within the data. Sensitivity analysis, on the other hand, validated the importance of each thematic map and the weights assigned to them, enhancing the overall credibility of the FRI map’s results. Together, these approaches improved the accuracy, reliability, and robustness of the FRI map, making it a valuable tool for flood risk assessment and management.

**Table 16** Villages and area mapping based on FRI classification

Types	Name of the village	Area (%)	Area (km)
Very low	Veragattam, Sarubujjili, Jalumuru, Heramandalam, Kotturu, Nandigam	8	467
Low	Ranastalam, Laveru, Srikakulam, Amadalavasa, Sompeta	28	1635
Medium	Hetchrla, Gara, Narasannapeta, kotabommali, Regidi amadalavalasa, Seetampeta, Bamini, Saravakota, Miliyaputti	16	934
High	Ganguvari sigadam, Santakaviti, Polaki, Santabommali, Palasa, Vagrapukotturu, Kanchili, Kaviti	20	1168
Very high	Vangara, Rajam, Palakonda, Burja, ponduru, Pathapatnam, Tekkali, Kusumala, Ichapuram	28	1636



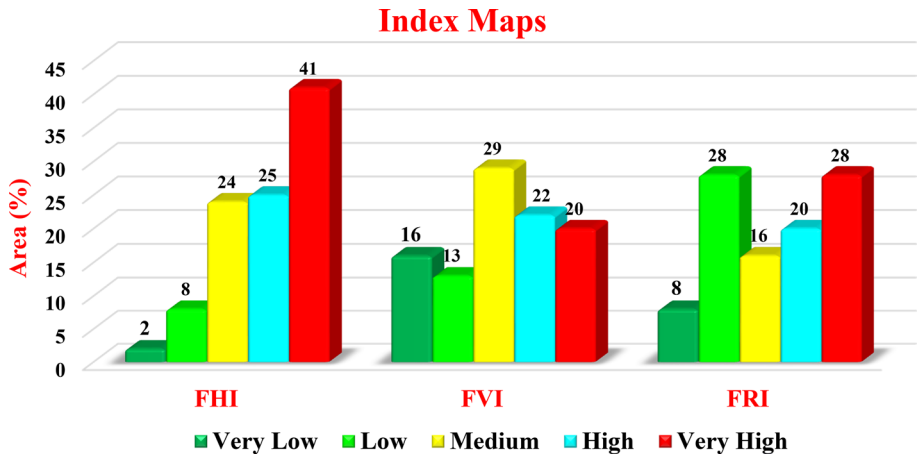


Fig. 24 Graph showing percentage of study area corresponding to FHI, FVI and FRI

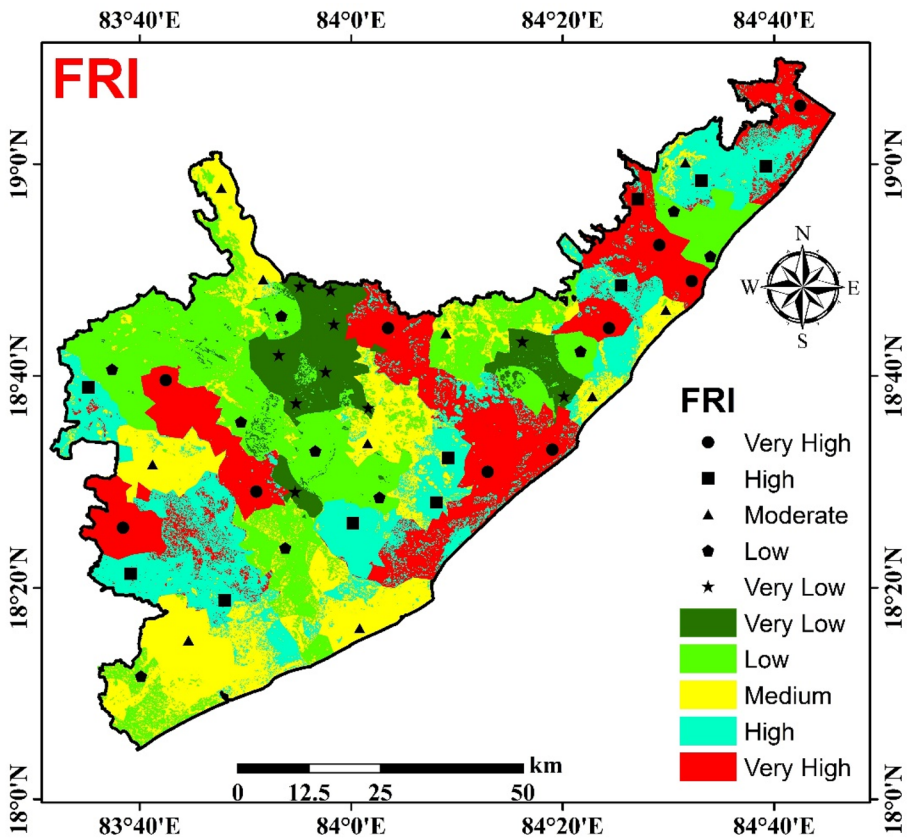
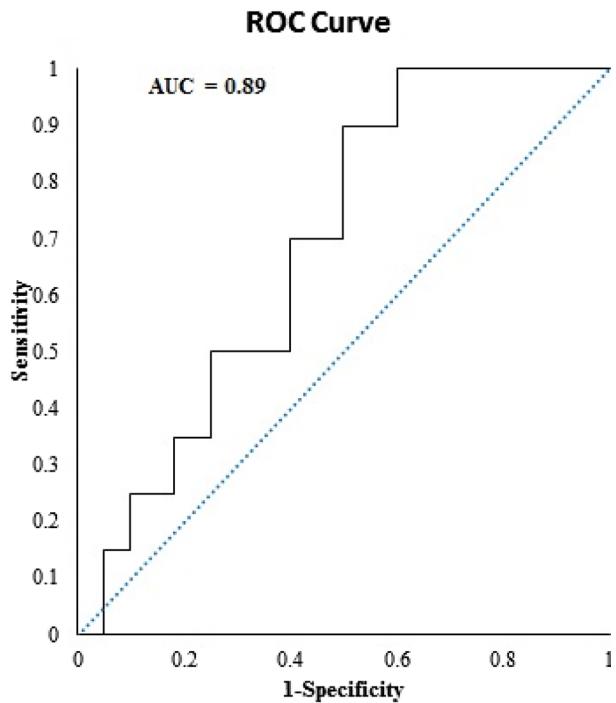


Fig. 25 FRI map with ground truth points

**Fig. 26** Cross-validation of the FRI map using ROC curve



**Author contribution** The author contributed to the study conception, design, material preparation, data collection and analysis. The first draft of the manuscript was written by Dr. Sanjay Ku. Ray. The author read and approved the final manuscript.

**Funding** No funding was obtained for this study.

**Data availability** The submitted article contains all of the data and models developed or utilized during the study. There is no separate data available with this manuscript.

## Declarations

**Conflict of interest** The authors declare that there is no known competing financial interests or personal relationships that could have appeared to influence the work reported in this paper. The author has no conflicts of interest to declare.

## References

- Abu El-Magd, S. A., Amer, R. A., & Embaby, A. (2020). Multi-criteria decision-making for the analysis of flash floods: A case study of Awlad Toq-Sherq, Southeast Sohag, Egypt. *Journal of African Earth Sciences*, 162, 103709. <https://doi.org/10.1016/j.jafrearsci.2019.103709>
- Amare, G. N., & Okubay, G. A. (2019). Flood hazard risk vulnerability mapping using Geo-spatial and MCDA around Adigrat, Tigray Region, Northern Ethiopia. *Momona Ethiopian Journal of Science*, 7(1), 90–107. <https://doi.org/10.4314/mejs.v11i1.6>
- Arrighi, C. (2021). A global scale analysis of river flood risk of UNESCO world heritage sites. *Frontiers in Water*, 3, 1–12. <https://doi.org/10.3389/frwa.2021.764459>

- Arya, A. K., & Singh, A. P. (2021). Multi criteria analysis for flood hazard mapping using GIS techniques: A case study of Ghaghara River basin in Uttar Pradesh, India. *Arabian Journal of Geosciences*, 14(8), 1–12. <https://doi.org/10.1007/s12517-021-06971-1>
- Baquedano, J. A. P., & Ferreira, T. M. (2021). From single- to multi-hazard vulnerability and risk in historic urban areas: A literature review. *Natural Hazards*, 108, 93–128. <https://doi.org/10.1007/s11069-021-04734-5>
- Bonazza, A., Maxwell, I., Drd, A. M., Vintzileou, E., & Hanus, C. (2018). Safeguarding cultural heritage from natural and manmade disasters—A comparative analysis of risk management in the EU. European Commission. <https://publications.europa.eu/en/publicationdetail/-/publication/8fe9ea60-4cea-11e8-be1d-01aa75ed71a1/language-en>
- Chakraborty, S., & Mukhopadhyay, S. (2019). Assessing flood risk using analytical hierarchy process (AHP) and geographical information system (GIS): Application in Coochbehar district of West Bengal, India. *Natural Hazards*, 99(1), 247–274. <https://doi.org/10.1007/s11069-019-03737-7>
- Chen, H., Liang, Z., Liu, Y., Jiang, Q., & Xie, S. (2018). Effects of drought and flood on crop production in China across 1949–2015: Spatial heterogeneity analysis with Bayesian hierarchical modeling. *Natural Hazards*, 92, 525–541. <https://doi.org/10.1007/s11069-018-3216-0>
- Dayala, D., Wang, K., Yan, Y., Smith, H., Massam, A., Filipova, V., & Jacqueline, P. J. (2020). Flood vulnerability and risk assessment of urban traditional buildings in a heritage district of Kuala Lumpur, Malaysia. *Natural Hazards and Earth System Sciences*, 20(8), 2221–2241. <https://doi.org/10.5194/nhess-20-2221-2020>
- Desalegn, H., & Mulu, A. (2020). Flood vulnerability assessment using GIS at Fetam watershed, upper Abbay basin, Ethiopia. *Heliyon*, 7, 05865. <https://doi.org/10.1016/j.heliyon.2020.e05865>
- Doorga, J. R. S., Magerl, L., Bunwaree, P., Zhao, J., Watkins, S., Staub, C. G., Rughooputh, S. D. D. V., Cundenn, T. S. M., Lollchund, R., & Boojhawon, R. (2022). GIS-based multi-criteria modelling of flood risk susceptibility in Port Louis, Mauritius: Towards resilient flood management. *International Journal of Disaster Risk Reduction*, 67, 102683. <https://doi.org/10.1016/j.ijdr.2021.102683>
- Ehteram, M., Ahmed, A. N., Chow, M. F., Latif, S. D., Chau, K. W., Chong, K. L., & El-Shafie, A. (2022). Optimal operation of hydropower reservoirs under climate change. *Environment, Development and Sustainability*, 25, 10627–10659. <https://doi.org/10.1007/s10668-022-02497-y>
- Ferreira, T. M., & Santos, P. P. (2020). An integrated approach for assessing flood risk in historic city centres. *Water*, 12(6), 1648. <https://doi.org/10.3390/w12061648>
- Gandini, A., Garmendia, L., Prieto, I., Alvarez, I., & San-Jose, J. T. (2020). A holistic and multi-stakeholder methodology for vulnerability assessment of cities to flooding and extreme precipitation events. *Sustainable Cities and Society*, 63, 102437. <https://doi.org/10.1016/j.scs.2020.102437>
- Gazi, Y., Islam, A., & Hossai, S. (2019). Flood-hazard mapping in a regional scale-way forward to the future hazard Atlas in Bangladesh. *Malaysian Journal Geosciences*, 3(1), 01–1. <https://doi.org/10.26480/mjg.01.2019.01.11>
- Hermas, E., Gaber, A., & Bastawesy, M. E. (2021). Application of remote sensing and GIS for assessing and proposing mitigation measures in flood-affected urban areas, Egypt. *The Egyptian Journal of Remote Sensing and Space Science*, 24(1), 119–130. <https://doi.org/10.1016/j.ejrs.2020.03.002>
- Hussain, M., Tayyab, M., Zhang, J., Shah, A. A., Ullah, K., Mehmood, U., & AlShaibah, B. (2021). GIS-Based multi-criteria approach for flood vulnerability assessment and mapping in district Shangla: Khyber Pakhtunkhwa Pakistan. *Sustainability*, 13, 3126. <https://doi.org/10.3390/su13063126>
- Khosravi, K., Shahabi, H., Pham, B. T., Adamowski, J., Shirzadi, A., Pradhan, B., Dou, J., Ly, H., Gróf, G., Ho, H. L., Hong, H., Chapi, K., & Prakash, I. (2019). A comparative assessment of flood susceptibility modeling using Multi-Criteria Decision-Making Analysis and Machine Learning Methods. *Journal of Hydrology*, 573, 311–323. <https://doi.org/10.1016/j.jhydrol.2019.03.073>
- Kienberger, S., Lang, S., & Zeil, P. (2009). Spatial vulnerability units: Expert-based spatial modelling of socio-economic vulnerability in the Salzach catchment, Austria. *Natural Hazards and Earth Systems Sciences*, 9, 767–778. <https://doi.org/10.5194/nhess-9-767-2009>
- Lai, V., Huang, Y. F., Koo, C. H., Ahmed, A. N., & El-Shafie, A. (2022). Conceptual Sim-Heuristic optimization algorithm to evaluate the climate impact on reservoir operations. *Journal of Hydrology*, 614(A), 128530. <https://doi.org/10.1016/j.jhydrol.2022.128530>
- Martinez-Gomariz, E., Forero-Ortiz, E., Russo, B., Locatelli, C., Guerrero-Hidalga, M., Yubero, D., & Castand, S. (2021). A novel expert opinion-based approach to compute estimations of flood damage to property in dense urban environments. Barcelona case study. *Journal of Hydrology*, 598, 126244. <https://doi.org/10.1016/j.jhydrol.2021.126244>
- Memon, N., Patel, D. P., Bhatt, N., & Patel, S. B. (2020). Integrated framework for flood relief package (FRP) allocation in semiarid region: A case of Rel River flood, Gujarat, India. *Natural Hazards*, 100, 279–311. <https://doi.org/10.1007/s11069-019-03812-z>

- Merz, B., Bloesch, G., Vorogushyn, S., Dottori, F., Aerts, J. C. J. H., Bates, P., Bertola, M., Kemter, M., Kreibich, H., Lall, U., & Macdonald, E. (2021). Causes, impacts and patterns of disastrous river floods. *Nature Reviews Earth and Environment*, 2(9), 592–609. <https://doi.org/10.1038/s43017-021-00195-3>
- Miranda, F. N., & Ferreira, T. M. (2019). A simplified approach for flood vulnerability assessment of historic sites. *Natural Hazards*, 96(2), 713–730. <https://doi.org/10.1007/s11069-018-03565-1>
- Montgomery, D. C., Peck, E. A., & Vining, G. G. (2013). *Introduction to Linear Regression Analysis* (5th ed.). New Jersey: Wiley.
- Morea, H., & Samanta, S. (2020). Multi-criteria decision approach to identify flood vulnerability zones using geospatial technology in the kemp-welch catchment, Central province. *Applied Geomatics*, 12(4), 427–440. <https://doi.org/10.1007/s12518-020-00315-6>
- Mundhe, N. (2019). Multi-criteria decision making vulnerability mapping of flood hazard: A case study Pune city. *Journal of Geographical Studies*, 2(1), 41–52. <https://doi.org/10.21523/gcj5.18020105>
- Nasiri, H., Mohd, Y. M. J., & Mohammad, A. T. A. (2016). An overview to flood vulnerability assessment methods. *Sustainable Water Resources Management*, 2(3), 331–336. <https://doi.org/10.1007/s40899-016-0051-x>
- Ogato, G. S., Bantider, A., Abebe, K., & Geneletti, D. (2020). Geographic information system (GIS)–based multi criteria analysis of flooding hazard and risk in Ambo Town and its watershed, West shoa zone, Oromia regional State Ethiopia. *Journal of Hydrology: Regional Studies*, 27, 100659. <https://doi.org/10.1016/j.ejrh.2019.10>
- Palacio-Aponte, A. G., Ortíz-Rodríguez, A. J., & Sandoval-Solis, S. (2022). Methodological framework for territorial planning of urban areas: Analysis of socio-economic vulnerability and risk associated with flash flood hazards. *Applied Geography*, 149, 102809. <https://doi.org/10.1016/j.apgeog.2022.102809>
- Petroselli, A., Vojtek, M., & Vojtekova, J. (2019). Flood mapping in small ungauged basins: A comparison of different approaches for two case studies in Slovakia. *Hydrology Research*, 50, 379–392. <https://doi.org/10.2166/nh.2018.040>
- Polong, F., Deng, K., Pham, Q. B., Linh, N. T. T., Abba, S. I., Ahmed, A. N., Anh, D. T., Khedher, K. M., & El-Shafie, A. (2023). Separation and attribution of impacts of changes in land use and climate on hydrological processes. *Theoretical and Applied Climatology*, 151, 1337–1353. <https://doi.org/10.1007/s00704-022-04351-7>
- Prieto, C., Patel, D., & Han, D. (2020). Preface: Advances in flood risk assessment and management. *Natural Hazards and Earth Systems Sciences*, 20, 1045–1048. <https://doi.org/10.5194/nhess-20-1045-2020>
- Quinn, N., Bates, P. D., Neal, J., Smith, A., Wing, O., Sampson, C., Smith, J., & Heffernan, J. (2019). The spatial dependence of flood hazard and risk in the United States. *Water Resources Research*, 55, 1–22. <https://doi.org/10.1029/2018WR024205>
- Ray, S. K. (2023). Identifying the groundwater potential zones in Jamsholaghat sub-basin by considering GIS and multi-criteria decision analysis. *International Journal of Environmental Science and Technology*. <https://doi.org/10.1007/s13762-023-04923-8>
- Requena, A. I., Ouarda, T. B. M. J., & Chebana, F. (2018). Low-flow frequency analysis at ungauged sites based on regionally estimated stream flows. *Journal of Hydrology*, 563, 523–532. <https://doi.org/10.1016/j.jhydrol.2018.06.016>
- Rincon, D., Khan, U. T., & Armenakis, C. (2018). Flood risk mapping using GIS and multi-criteria analysis: A greater Toronto area case study. *Geosciences*, 8, 275. <https://doi.org/10.3390/geosciences8080275>
- Saaty, R. W. (1987). The analytic hierarchy process—what it is and how it is used. *Mathematical Modeling*, 9, 161–176. [https://doi.org/10.1016/0270-0255\(87\)90473-8](https://doi.org/10.1016/0270-0255(87)90473-8)
- Saaty, T. L. (1990). How to make a decision: The analytic hierarchy process. *European Journal of Operational Research*, 48, 9–26. [https://doi.org/10.1016/0377-2217\(90\)90057-1](https://doi.org/10.1016/0377-2217(90)90057-1)
- Saaty, T. L. (2008). Decision making with the analytic hierarchy process. *International Journal of Services Sciences*, 1(1), 83–98. <https://doi.org/10.1504/IJSSCI.2008.017590>
- Samela, C. R., Sole, A., & Manferda, S. (2018). A GIS tool for cost-effective delineation of flood-prone areas. *Computers, Environment and Urban Systems*, 70, 43–52. <https://doi.org/10.1016/j.compenvurbys.2018.01.013>
- Schroeder, A. J., Gourley, J. J., Hardy, J., Henderson, J. J., Parhi, P., Rahmani, V., Reed, K. A., Schumacher, R. S., Smith, B. K., & Taraldsen, M. J. (2016). The development of a flash flood severity index. *Journal of Hydrology*, 541(A), 523–532. <https://doi.org/10.1016/j.jhydrol.2016.04.005>
- Shahabi, H., Shirzadi, A., Ronoud, S., Asadi, S., Pham, B. T., Mansouripour, F., Geertsema, M., Clague, J. J., & Bui, D. T. (2021). Flash flood susceptibility mapping using a novel deep learning model based on deep belief network, back propagation and genetic algorithm. *Geoscience Frontiers*, 12(3), 101100. <https://doi.org/10.1016/j.gsf.2020.10.007>

- Singh, A. P., Arya, A. K., & Singh, D. S. (2020). Morphometric analysis of Ghaghara River basin, India, using SRTM data and GIS. *Journal of the Geological Society of India*, 95(2), 169–178. <https://doi.org/10.1007/s12594-0201406-3>
- Solomon, M. K., Ferreira, C. S. S., Zupanc, V., Ristic, R., Drobnyak, A., & Kalantari, Z. (2021). Flood legislation and land policy framework of EU and non-EU countries in Southern Europe. *WIREs*, 9(1), e1566. <https://doi.org/10.1002/wat2.1566>
- Teng, J., Jakeman, A. J., Vaze, J., Croke, B. F. W., Dutta, D., & Kim, S. (2017). Flood inundation modelling: A review of methods, recent advances and uncertainty analysis. *Environmental Modelling and Software*, 90, 201–216. <https://doi.org/10.1016/j.envsoft.2017.01.006>
- Velasco, M., Cabello, À., & Russo, B. (2016). Flood damage assessment in urban areas. Application to the Raval district of Barcelona using synthetic depth damage curves. *Urban Water Journal*, 13, 426–440. <https://doi.org/10.1080/1573062X.2014.994005>
- Vojtek, M., & Vojtekova, J. (2019). Flood susceptibility mapping on a national scale in Slovakia using the analytical hierarchy process. *Water*, 11, 364. <https://doi.org/10.3390/w11020364>
- Vörösmarty, C. J., Lévêque, C., Revenga, C., Bos, R., Caudill, C., Clinton, J., Douglas, E. M., Nilsson, C., Oki, T., Reidy, C. A., Rijsberman, F., Costanza, R., & Jacobi, P. (2005). Fresh water. In R. Hassan, R. Scholes, & N. Ash (Eds.), *Ecosystems and human well-being: current state and trends* (Vol. 1, p. 917). Washington DC: Millennium Ecosystem Assessment.
- Xiao, S., Li, N., & Guo, X. (2021). Analysis of flood impacts on masonry structures and mitigation measures. *Journal of Flood Risk Management*, 14(4), e12743. <https://doi.org/10.1111/jfr3.12743>
- Yang, W., Xu, K., Lian, J., Ma, C., & Bin, L. (2018). Integrated flood vulnerability assessment approach based on TOPSIS and Shannon entropy methods. *Ecological Indicators*, 89, 269–280. <https://doi.org/10.1016/j.ecolind.2018.02.015>

**Publisher's Note** Springer Nature remains neutral with regard to jurisdictional claims in published maps and institutional affiliations.

Springer Nature or its licensor (e.g. a society or other partner) holds exclusive rights to this article under a publishing agreement with the author(s) or other rightsholder(s); author self-archiving of the accepted manuscript version of this article is solely governed by the terms of such publishing agreement and applicable law.